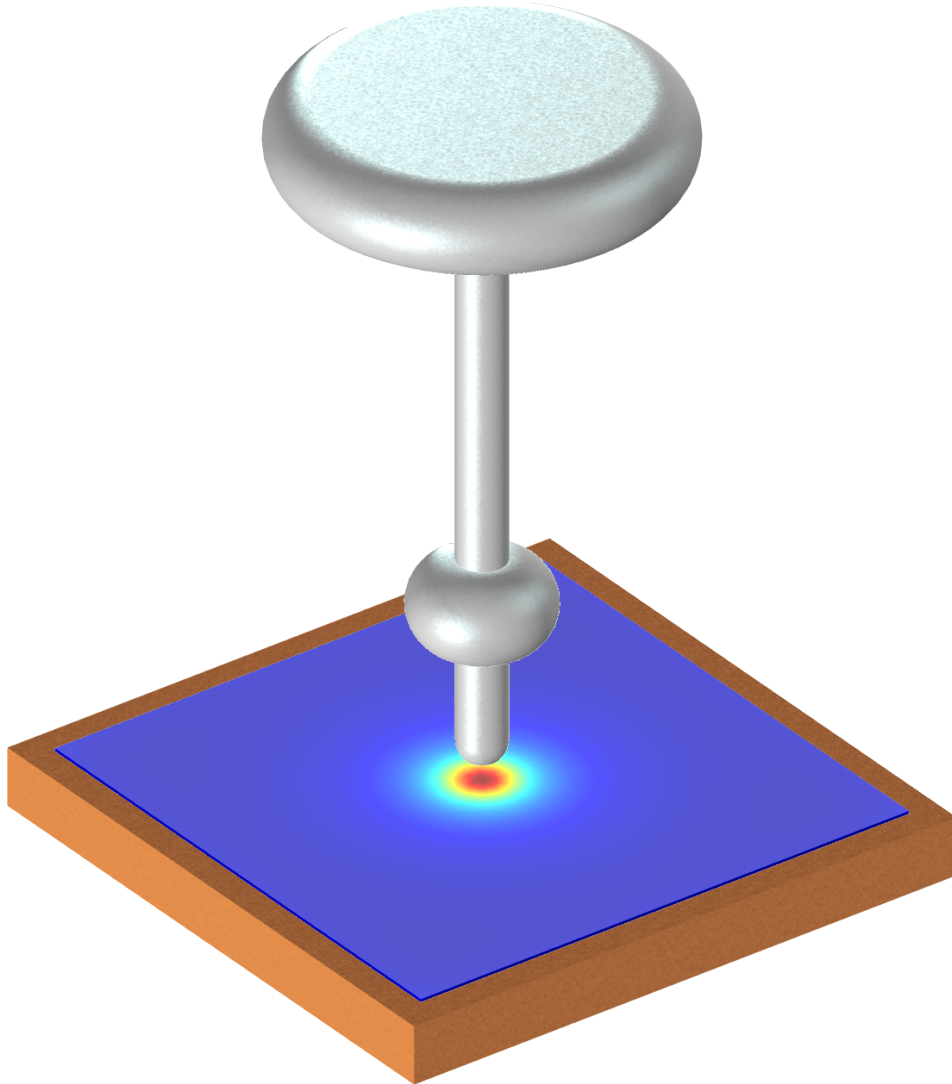




CHALMERS
UNIVERSITY OF TECHNOLOGY



Humidity Dependence of Charge Accumulation on Polymer-Air Interfaces for HVDC Applications

Master's Thesis in Electric Power Engineering

DANIEL SVENSSON

Department of Electrical Engineering
Chalmers University of Technology
Gothenburg, Sweden 2021

MASTER'S THESIS IN ELECTRIC POWER ENGINEERING

Humidity Dependence of Charge Accumulation on Polymer-Air Interfaces for HVDC Applications

DANIEL SVENSSON



Division of Electric Power Engineering
Department of Electrical Engineering
CHALMERS UNIVERSITY OF TECHNOLOGY
Gothenburg, Sweden 2021

Humidity Dependence of Charge Accumulation on Polymer-Air Interfaces for HVDC Applications

© DANIEL SVENSSON, 2021.

Supervisors: Adj. Prof. Olof Hjortstam, Hitachi ABB Power Grids Research;
Ph.D. Sarath Kumara, Chalmers University of Technology
Examiner: Prof. Yuriy Serdyuk, Chalmers University of Technology

Master's Thesis 2021
Division of Electric Power Engineering
Department of Electrical Engineering
Chalmers University of Technology
SE-412 96 Gothenburg
Telephone +46 31 772 1000

Cover: 3D model of an electrode setup for surface charging of flat polymeric samples.

Typeset in L^AT_EX
Printed by Chalmers Reproservice
Gothenburg, Sweden 2021

Humidity Dependence of Charge Accumulation on Polymer-Air Interfaces for HVDC Applications

Daniel Svensson

Division of Electric Power Engineering
Department of Electrical Engineering
Chalmers University of Technology

Abstract

Polymeric insulators immersed in air are widely used in high voltage direct current (HVDC) applications. In operation, they are continuously exposed to static electric fields, which impose electrostatic forces on ionic species present in the surrounding air causing their directional motion. While drifting in the field, the ions arrive to solid insulators surfaces and accumulate on them over time resulting in local field variations. The performed research have indicated that these field variations may have a detrimental effect on insulation performance. Thus, understanding factors that influence surface charge accumulation is of great importance for proper design of HVDC insulators. One of such factors is moisture in air. It has previously been demonstrated that the electric conductivity of air increases exponentially with humidity and thus it can be expected that the rate of surface charge accumulation also increases with humidity. Therefore, it is of practical interest to investigate the humidity dependence of charge accumulation on polymer-air interfaces. Accordingly, the focus of this thesis is to identify such a dependence by investigating electrostatic potential on the surface of a flat polymeric sample induced by deposited charges under various levels of humidity.

An experimental setup allowing for surface charging and surface potential measurements on flat material samples under different levels of humidity has been developed. In the experiments, a flat sample of polytetrafluoroethylene (Teflon) was used. It was placed on a grounded copper plate and its open surface was charged. The charging was implemented by applying high voltage to a rod electrode placed above the sample. The electrodes with the sample were placed in a sealed box inside which the humidity of air was controlled by using different saturated salt solutions. The magnitude of the charging voltage was chosen to be below the onset voltage of electron avalanches to avoid an excess amount of charged species in air. The experiments were conducted with both a positive and negative test voltage of 4 kV which was applied for 4 hours to allow for sufficient charging of the sample. The relative humidity levels of air were 21, 40, 51, 70, 90 and 98% at 20°C. The electric potentials of the charged surface—measured with a capacitive probe—were converted into corresponding surface charge densities through electrostatic field equations. According to the experimental results, it was found that the initial charging rate increased exponentially with relative humidity for both polarities being substantially greater in the case of positive polarity. Furthermore, a significant expansion of the deposited charges over the sample surface was observed for higher humidity levels. The reasons for this effect are discussed in terms of surface conduction associated with the presence of secondary charged regions altering the tangential electric field.

Acknowledgements

First, I want to thank my supervisor Sarath Kumara at Chalmers who has helped me tremendously throughout this project. His expertise in charging of polymeric surfaces has been particularly useful along with his feedback and suggestions. I also appreciate that he showed a great interest in my topic and seemed happy whenever I came to visit him to discuss something or share ideas.

I also want to thank my supervisor Olof Hjortstam at Hitachi ABB Power Grids Research who helped guide the thesis in the right direction and suggested ways forward. His positive attitude and kind words of encouragement always made me look forward to our meetings which I found to be very helpful and productive.

Finally, many thanks to my examiner Yuriy Serdyuk for providing me this great opportunity and interesting thesis within high voltage engineering. He is someone who gladly helps with explaining complex physical phenomena and does not seem bothered when students ask many questions, in fact quite the opposite. It clearly shows that he has a passion for teaching, and for that I am grateful to have him as my examiner.

Daniel Svensson, Gothenburg, June 2021

Table of contents

1	Introduction	1
1.1	Background	1
1.2	Problem statement	2
1.3	Purpose	2
1.4	Objectives	2
2	Literature review	5
2.1	Naturally occurring charge carriers in air	5
2.2	Electric field dependence of electric currents in air	6
2.2.1	Uniform electric field	7
2.2.2	Non-uniform electric field	9
2.3	Concept and control of humidity	10
2.4	Surface charge accumulation	12
2.5	Surface charge decay	14
2.6	Field-nullifying method for non-contact surface potential measurements	15
2.7	Ion emission from water adsorbed onto metal surfaces under high electric fields	16
3	Method	19
3.1	Experimental setup	19
3.2	Experimental procedure	21
3.3	Simulation of electrostatic field in Comsol Multiphysics	22
3.3.1	Electrostatics - governing equations	22
3.3.2	Model implementation	23
3.3.3	Solution	25
4	Results and discussion	27
4.1	Humidity dependence	27
4.1.1	Negative polarity	27
4.1.2	Positive polarity	31
4.2	Charge distribution	34
5	Conclusions	37
6	Future Work	39
	References	42

1 Introduction

This thesis seeks to explore the humidity dependence of charge accumulation on polymer-air interfaces for high voltage direct current (HVDC) applications. More specifically, it aims to study the surface charging of a flat polytetrafluoroethylene (Teflon) sample—below the electron avalanche onset voltage—for a wide range of humidity using both a positive and negative voltage. It is a part of a collaborative research project between Chalmers and Hitachi ABB Power Grids Research (PGR) referred to as “Charge dynamics in future HVDC insulation systems” with the partial aim of improving the design of insulation systems to withstand higher voltage levels. As such, the experimental results and conclusions from this thesis are intended to serve as input towards that project. This chapter begins with an overview of the background that frames the thesis. Following this is the problem statement which illustrates the reason why the study should be conducted—why it is important. Then comes the thesis’s purpose, and finally, a specification of the objectives required to fulfill it.

1.1 Background

HVDC technology provides an efficient way for transporting large amount of electrical power over long distances—utilizing DC for the bulk transmission. Consequently, HVDC transmission systems are actively being developed in countries where energy sources are located far away from load centers, such as China where voltage levels up to 1100 kV was recently commissioned [1]. To ensure a secure and reliable operation of such systems, components with different electric potentials need to be sufficiently electrically insulated from each other to avoid unexpected flashover events, and hence, high demands are put on materials used for electrical insulation. Regarding outdoor installations of HVDC systems, insulators based on composite polymeric materials are primarily used due to numerous technical advantages compared to traditionally used insulators based on glass and porcelain [2]. Consequently, polymeric insulators must be able to function even under large fluctuations of the surrounding meteorological environment.

Under HVDC conditions, an electrical insulator is continuously stressed with a DC electric field which spreads out into the surroundings as depicted in figure 1.1. This static field then drives charges which appear naturally in the air (section 2.1) along its field lines towards the insulator, resulting in an accumulation of charge on its surface. As the electric field from these charges is superimposed onto the background electric field, local field variations in the total electric field occur which could possibly cause a deterioration of the insulation performance [3]. Regarding the design of electrical insulators, an accurate representation of the electric field is crucial. Therefore, understanding factors that influence surface charge accumulation is greatly beneficial for a proper design of electrical insulators intended to HVDC applications.

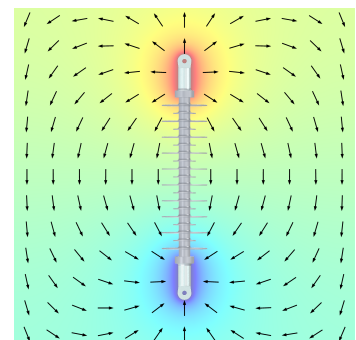


Figure 1.1: Electric field from a polymeric insulator.

In a recent master's thesis work at Hitachi ABB PGR it was found that the current between two parallel plate electrodes in air energized within 0.5–2 kV/mm was heavily dependent on humidity; increasing exponentially with increasing moisture levels [4]. Although the reason for this dependency is not yet fully understood, it is believed that the increase of current is due to an electrochemical reaction taking place in water clusters on the electrode surface, which then results in the emission of extra charges (water ion clusters) [5]. With this in mind, it is expected that surface charging under high humidity is different than in dry air, which may affect insulation performance.

1.2 Problem statement

Research indicate that surface charge accumulated on polymeric insulators can have a detrimental effect on insulation performance [3]. As air conductivity is greatly affected by humidity, it is expected that surface charge accumulation is different under humid conditions [4]. If such is the case, it follows that insulation performance is also different, and thus, could potentially promote conditions for an electrical breakdown. Therefore, it is of interest to study how humidity potentially affects the accumulation of charges on insulator surfaces.

1.3 Purpose

The main idea of this thesis is to carry out an experimental study to examine the build-up of surface charge on a polymeric insulating material—under HVDC conditions—and how it depends on the concentration of water vapor in the surrounding air. The purpose is to identify and explain this dependency in a general sense along with the physical mechanisms responsible. A better understanding of this phenomena is crucial input to an optimal and reliable design of HVDC insulation systems, and will thus lead to more informed decisions being made during the design process of these systems intended for humid environments.

1.4 Objectives

To realize the above mentioned purpose, a flat sample of a polymeric insulation material—in this case Teflon—shall have its surface charged. The reason for choosing Teflon here is because it fits the requirement of having a low bulk conductivity, thereby limiting the rate at which charges on the surface decay through the bulk of the material; allowing them to be studied more easily. The charging is to be done by energizing an electrode positioned above the sample while having another electrode below it that is grounded, causing surrounding charges to drift towards the sample's surface due to the resulting electric field. For simplicity, the electrode will be energized below the onset voltage for electron avalanches, thereby eliminating the possibility for charge to be generated by impact ionization (see 2.2.1). With there being fewer mechanisms of charge generation involved, further investigation of the hypothesis that charges are emitted from water clusters on the electrode surface is greatly simplified. This, however, requires knowledge about the onset voltage for avalanche development, hence it shall be estimated by performing computer simulations of the electrostatic field around the electrode.

Regarding surface charge on the charged sample, it can be determined from corresponding surface potential. As surface potential is proportional to surface charge density for flat samples, converting between these two quantities is quite straightforward [3]. In accordance with the purpose, the charging should be conducted for a wide range of humidity. However, there is another parameter whose impact on the charging is of interest to investigate as well, namely, the polarity of the voltage applied to the electrode. It is expected that emission of water ion clusters is also polarity dependent since negative water ion clusters differ from positive ones. If such is the case, it could provide further evidence towards the above mentioned mechanism of charge generation, hence it is of interest to examine. Finally, as this thesis is of an experimental nature it requires the development of an experimental setup. The setup should allow for surface charging of flat polymeric samples in an environment where the humidity is measured and regulated. In addition to this it should be able to measure surface potential. In summary, the objectives are as follows:

- Develop an experimental setup that can charge surfaces of flat polymeric samples, measure surface potential as well as monitor and regulate humidity.
- Calculate onset voltage for electron avalanches for given electrode arrangement using Comsol Multiphysics software.
- Conduct surface charging experiments and surface potential measurements—below onset voltage for electron avalanches—while varying humidity and voltage polarity.
- Identify and attempt to explain any humidity dependence on surface charge accumulation along with the polarity of the applied voltage.

2 Literature review

This chapter presents a review of literature related to the thesis topic with the intention to provide a brief understanding of important background theory as well as an overview of related previous studies. It begins with an explanation of why air naturally contains a certain amount of free electric charge. After that, the relationship between electric field and current in air is covered. Then comes some general information on humidity and how it can be controlled. Next, the process that accounts for surface charge accumulation is covered along with a brief description of its decay mechanisms. It also covers the operational principle of a method for measuring surface potential and how it can be converted into corresponding surface charge. Finally, it finishes with an exposition of the idea that water ions are emitted from electrode surfaces under influence of high surface electric fields and how it is in agreement with previous studies.

2.1 Naturally occurring charge carriers in air

Charge carriers are particles that are free to move and carry an electric charge. Examples being free electrons and ions—where ions are atoms or molecules with a net electric charge. The process through which a neutral atom or molecule becomes an ion by acquiring or releasing electrons is known as ionization. It turns out that the atmospheric air is continuously ionized by different types of naturally occurring radiation, which primarily consists of cosmic rays (originating from the sun and deep space) and decay of radioactive substances in the ground and in the air [6]. This results in the generation of positive ions and free electrons as nitrogen N_2 and oxygen O_2 are broken up into N_2^+ and O_2^+ , respectively [7], which is illustrated in figure 2.1. In turn, the free electrons rapidly attach to nearby highly electronegative neutral air molecules, forming negative ions (N_2^- and O_2^-).

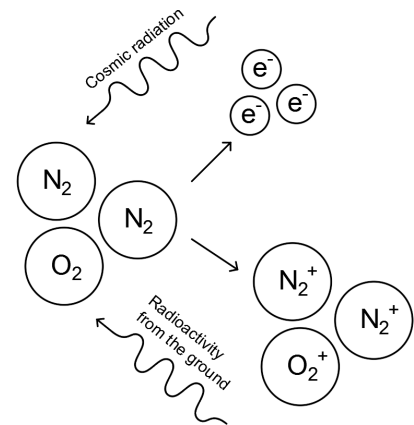


Figure 2.1: Natural ionization of air.

Thus, in order to cause ionization in air, chemical bonds need to be broken which requires a relatively high amount of energy, namely, about 13.6 eV for oxygen and 14.5 eV for nitrogen. As the energy supplied by all types of radiation from a point source drops off with the square of the distance from the source, the rate of ionization vary greatly depending on location. In continental areas, the average rate of ionization is found to be about $10 \text{ ion pairs cm}^{-3}\text{s}^{-1}$ at surface level [8].

As positive and negative ions mix throughout the air, there is a chance they meet and collide with each other due to attractive Coulomb forces between them. When this happens, the extra electron in the negative ion is picked up by the positive ion, resulting in two neutral air molecules. This process thereby reduces the amount of charge carriers in the air and is referred to as recombination. The rate at which recombination occurs depends on the concentration of ion pairs; the higher the concentration, the more likely a recombination is to take place. Therefore, as more and more ion pairs are generated, the rate of recombination increases. Eventually, the

rate of recombination equals the rate of ionization, meaning that the concentration of ion-pairs remains constant. Thus, there exist a stationary equilibrium between the ion production and recombination process. This can be illustrated with an intuitive ion balance equation describing the rate of change of ion-pair concentration n [cm^{-3}] as

$$\frac{dn}{dt} = q - \alpha n^2 \quad (2.1)$$

where q is the average rate of ionization and α is the recombination coefficient, which has an average value of about $1.5 \cdot 10^{-6} \text{ cm}^3\text{s}^{-1}$ [8]. For n^+ and n^- positive and negative ions, respectively, the rate at which they recombine is proportional to the product $n^+ n^- = n^2$, with the proportionality constant α . Accordingly, the negative term represents the rate of recombination. For a constant ion-pair concentration, the term dn/dt becomes zero and the rate of ionization equals the rate of recombination, that is, $q = \alpha n^2$. Solving for n while neglecting the negative solution yields an ion pair concentration of $n = \sqrt{q/\alpha} \approx 2600 \text{ cm}^{-3}$ at steady-state. It should be noted that equation 2.1 assumes that the concentration of positive and negative charge is equal. This is not entirely true because of the so called atmospheric electrode effect, which causes there to be about 12 % more positive than negative charges at sea level [9]. Nonetheless, it still serves as a convenient way for estimating the amount of charge carriers in air that occur naturally.

Ions can also attach to aerosols which are particles suspended in air, such as dust, mist and fog. This establishes a charge distribution on the aerosol particle, resulting in so-called aerosol ions which are much larger in size, and therefore less mobile. Aerosols are hygroscopic meaning that they can absorb moisture from the atmosphere [10]. This property causes their size to increase as the concentration of water vapor increases. The larger size makes them more likely to attach to the much smaller initially generated ions, thereby reducing the amount of mobile charge carriers. This in turn reduces the conductivity of the air which is discussed in the next section.

2.2 Electric field dependence of electric currents in air

Under the influence of an electric field, charge carriers in air begin to accelerate and drift along electric field lines because of Coulomb forces exerted upon them. Positive charges drift in the direction of the field whereas negative charges drift in the opposite direction. The movement of charges in a volume of air can be equated to a volume current density, which is defined in the following analysis. Consider one type of charge carriers—each with a charge q —moving with a drift velocity \vec{v} , then for a time Δt each charge carrier moves a distance $\vec{v}\Delta t$. Now, consider an element of surface Δs whose normal vector \vec{a}_n is at an angle θ offset to the drift velocity, see figure 2.2. If N represents the volume density of charge carriers, the amount of charge ΔQ passing through the surface Δs is

$$\Delta Q = Nq\vec{v} \cdot \vec{a}_n \Delta t \Delta s \quad [\text{C}], \quad (2.2)$$

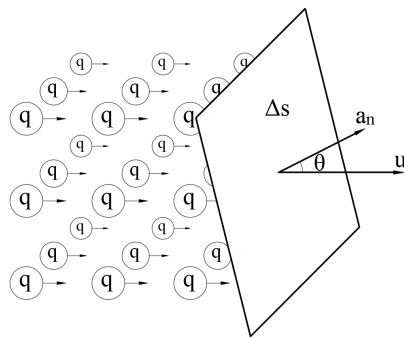


Figure 2.2: Charge carriers drifting through an imaginary surface.

where $\vec{v} \cdot \vec{a}_n = |\vec{v}| \cdot 1 \cos \theta$ extracts the component of the drift velocity perpendicular to the surface. Since electric current is defined as the rate of change of charge, that is $i(t) = \frac{dQ}{dt}$, equation 2.2 can be rearranged to express the average current ΔI over a time Δt as

$$\Delta I = \frac{\Delta Q}{\Delta t} = Nq\vec{v} \cdot \vec{a}_n \Delta s = Nq\vec{v} \cdot \Delta \vec{s} \quad [\text{A}]. \quad (2.3)$$

From this, a volume current density \vec{J} can be defined as the amount of current per *square* meter,

$$\vec{J} = \frac{\Delta I}{\Delta \vec{s}} = Nq\vec{v} = \rho\vec{v} \quad [\text{A}/\text{m}^2] \quad (2.4)$$

where ρ [C/m^3] is the free charge per unit volume. Note that if the charges drift along a surface instead, it equates to a surface current density with the unit [A/m]. With the definition of volume current density out of the way, its electric field dependence can now be discussed for a uniform as well as a non-uniform electric field in air.

2.2.1 Uniform electric field

The electric field dependence of electric currents in air was initially investigated by Townsend for a uniform electric field utilizing parallel plate electrodes [11], (figure 2.3). He found that the relationship between the current across the gap and the applied electric field falls into three distinct regions, namely, the ohmic region, the saturation region and the avalanche region, which is illustrated qualitatively in figure 2.4. From the figure it can be seen that the current increases linearly in the ohmic region, stays constant throughout the saturation region while increasing rapidly in the avalanche region. The reasons why the current behaves in this manner throughout the different regions is given below.

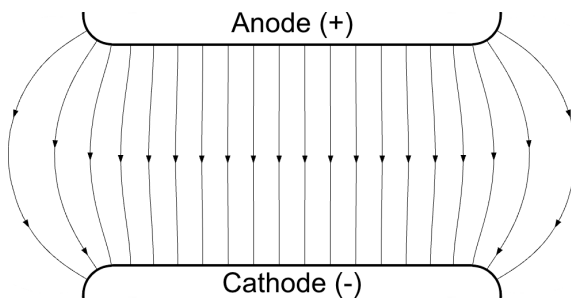


Figure 2.3: Electric field lines for a parallel plate gap.

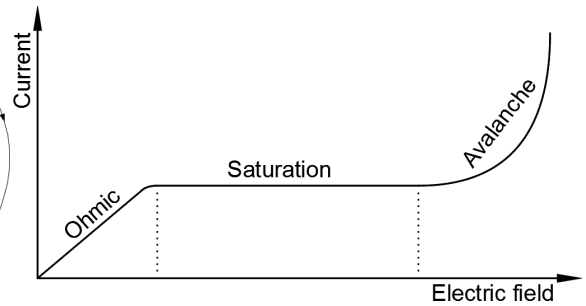


Figure 2.4: General pattern of the relationship between current and electric field for a parallel plate gap.

Ohmic region

As previously mentioned, a current is initiated when charge carriers are set in motion by an electric field. From Newton's second law of motion and the definition of electric field intensity, the equation describing their motion (in a classical manner) is

$$\left. \begin{array}{l} \vec{F} = m\vec{a} \\ \vec{F} = q\vec{E} \end{array} \right\} \rightarrow m \frac{d\vec{v}}{dt} = q\vec{E}, \quad (2.5)$$

with the solution

$$\vec{v}(t) = \frac{q\vec{E}t}{m} \quad [\text{m/s}]. \quad (2.6)$$

That is, an accelerated drift velocity directly proportional to the electric field intensity. As charge carriers drift through the air they inevitably collide with other particles causing a reduction of their accumulated velocity. For simplicity, an average drift velocity \vec{v} can be considered by assuming that the drift motion is completely lost in a collision and that the average time between collisions is τ , which is inversely proportional to the gas density and the size of the charge carriers.

$$\vec{v} = \frac{q\vec{E}\tau}{m} \quad [\text{m/s}]. \quad (2.7)$$

It is convenient to combine the factors $q\tau/m$ in equation 2.7 into a single factor μ [$\text{m}^2/(\text{Vs})$] as this results in a simple relation between the average drift velocity and the magnitude of the electric field

$$\vec{v} = \mu\vec{E} \quad [\text{m/s}]. \quad (2.8)$$

Here, μ is referred to as the mobility of the charge carriers and is a measure of a particle's ability to move through a medium in response to an electric field. Combining equations 2.8 and 2.4 yields a direct relation between the volume current density and the electric field known as the point form of Ohm's law [12]

$$\vec{J} = \rho\mu\vec{E} = \sigma\vec{E} \quad [\text{A/m}^2], \quad (2.9)$$

where σ [S/m] is the conductivity; a macroscopic property of the medium which quantifies how strongly it conducts electric current. For a medium containing multiple types of charge carriers—each with their respective concentration, mobility and polarity—the total conductivity of the medium can be expressed as

$$\sigma = \sum_i \rho_i^+ \mu_i^+ + \sum_i \rho_i^- \mu_i^- \quad [\text{S/m}] \quad (2.10)$$

where subscript i denotes the type of charge carrier. If the conductivity is constant (which is the case for an unchanging homogeneous medium) equation 2.9 results in a linear relationship between the current and the electric field with the slope being dictated by the conductivity. This explains the linearity in the ohmic region as air is indeed a homogeneous mixture.

Saturation region

If the electric field keeps increasing, the charge carriers kinetic energy increases accordingly, and eventually, it is high enough to overcome the attractive lower energy states associated with recombination. In other words, the force applied to the charge carriers by the electric field is greater than the attractive force between charge carriers of different polarity. This means that no recombination takes place and the initially generated charge carriers (electrons and positive ions) are all swept across the gap. Furthermore, for electric field strengths within this region,

the time required for charge carriers to drift across the gap is much shorter than the average time it takes for charge carriers to be generated. Therefore, the number of charge carriers reaching their corresponding electrode per unit time (the current) is limited by the rate at which these appear, that is, the rate of ionization. Since the rate of ionization is constant, it follows that the current is constant here as well.

Avalanche region

As the electric field increases even further, free lightweight electrons generated around the cathode (primary electrons) can accumulate enough kinetic energy between collisions with heavier gas molecules (due to conservation of momentum) as they drift towards the anode to eventually cause ionizing collisions. This liberates additional electrons which can also accumulate enough kinetic energy to cause further ionizing collisions, thereby releasing more and more electrons. This process can escalate very rapidly in an avalanche-like manner, resulting in an increasing number of charge carriers from the cathode to the anode, referred to as an *electron avalanche*, see figure 2.5. In turn, the corresponding positive ions drift toward the cathode where they then release electrons from its surface due to the direct energetic interaction between the ions and the surface atoms. This is a type of feedback process which provides secondary electrons at the cathode to act as new primary electrons for the next avalanche. If every avalanche causes at least one subsequent avalanche, a conductive channel is formed between the electrodes and the air breaks down, which equates to a huge inrush of current. From experiments it is found that for avalanche growth to take place in air the electric field needs to be at least 24.4 kV/cm for standard atmospheric conditions [13].

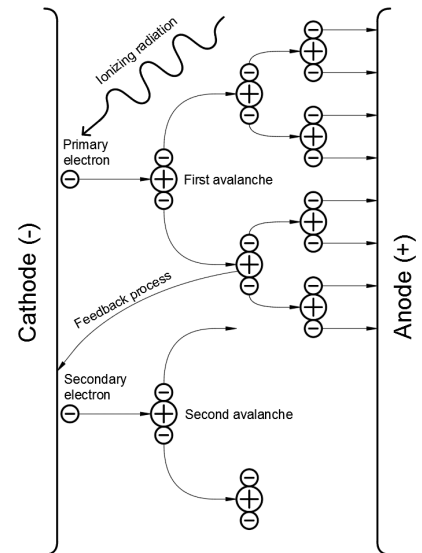


Figure 2.5: Development process of electron avalanches.

2.2.2 Non-uniform electric field

For a different type of electrode setup—such as a rod to plane gap—the electric field is non-uniform meaning that it varies across the gap (figure 2.6). This means that different parts of the gap can operate within different regions of the current-electric field characteristic. For instance, the volume close to the curved electrode surface where the electric field is particularly high could be within the avalanche region, while a different part of the gap where the field is lower could be within the saturation region. This means that as the applied voltage increases, avalanches initially start to develop in a very small volume around the highly curved electrode. As they propagate into the low-field region, there is no longer enough force applied to the electrons to cause further ionizing collisions, hence the

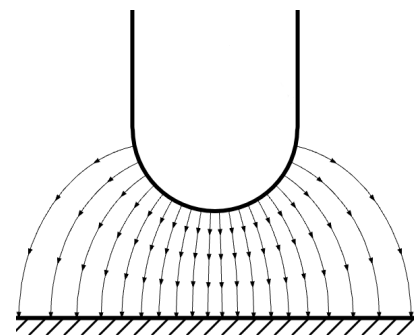


Figure 2.6: Electric field lines for a rod to plane gap.

avalanches begin to fade away. This phenomena is known as a pre-discharge (corona discharge), which is a partial discharge that does not cause a direct breakdown.

As the voltage increases even more, the volume where avalanche growth is possible increases accordingly, thereby increasing the amount of generated space charges around the electrode. Eventually, the amount of space charge is so high that its electric field distorts the background field in such a way that the total field is enhanced in front of the avalanches. This has to do with the way charge is distributed across an avalanche. Highly mobile electrons form a negative spherical avalanche head while the comparatively immobile positive ions form an avalanche tail. The electric field in front of the negative head has the same direction as the background field, meaning that the field at that point is enhanced, see figure 2.7. This then enables avalanches to propagate across the gap which could lead to an electrical breakdown due to a so-called streamer discharge.

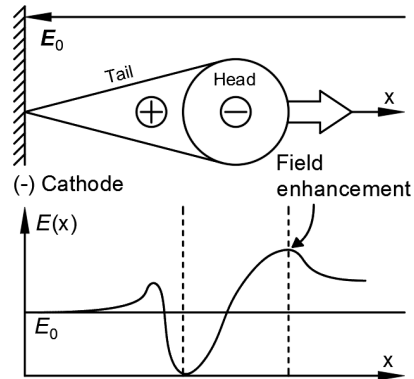


Figure 2.7: Distortion of the background electric field due to space charges of an electron avalanche.

Whether pre-discharges occur or not as the applied voltage increases clearly depends on the degree of non-uniformity of the electric field. This can be quantified by a factor η called the *field efficiency factor* defined as the ratio between the mean field intensity E_0 between the electrodes and the maximum field intensity E_{max} in the given electrode arrangement.

$$\eta = \frac{E_0}{E_{max}} = \frac{V}{dE_{max}} \quad (2.11)$$

The mean field of any electrode setup with a gap distance d is simply equal to the field intensity for a parallel-plate setup with the same distance, in other words $E_0 = V/d$. In a uniform field $\eta = 1$ since $E_{max} = E_0$ whereas in a strongly non-uniform field $E_{max} \gg E_0$ and $\eta \ll 1$. It turns out that a field efficiency factor below $\eta \approx 0.2$ is a prerequisite for pre-discharges to occur in standard atmospheric conditions [13]. Above this value there is no discrepancy between the voltage required for pre-discharges and the voltage required for total breakdown.

2.3 Concept and control of humidity

Humidity is a broad term that refers to the amount of water vapor present in the air. It can be expressed in different ways using different types of humidity. One way is to express it in absolute terms (absolute humidity) which simply indicates the mass of water vapor per unit volume of air as g/m^3 . Another way is to express it in relative terms known as relative humidity (RH). This type of measure gives the density of water vapor for a certain temperature *relative* to the maximum possible density of water vapor there could be at that temperature—expressed as a percentage. This measure makes sense to use if the temperature stays constant as the humidity changes. That way, all measures of humidity are relative to the same temperature and can thus easily be compared. However, if the temperature changes it is generally better to use absolute humidity as this measure is independent of the temperature.

The amount of water vapor depends on the temperature and the amount of available water. For the same amount of available water, warm air generally contains more water vapor than cold air. This is simply because the rate at which water molecules evaporate increases with temperature. Keep in mind that temperature is a measure of the *average* kinetic energy of a substance, meaning that the substance's particles don't all have the same kinetic energy. In fact, the velocities of the particles fall under a certain distribution of velocities that changes with the temperature—illustrated qualitatively in figure 2.8. For the case of water, this means that some molecules will have enough kinetic energy to evaporate even though the temperature is below the evaporation point. Similarly, if the temperature is above the evaporation point, some water molecules will still not have enough kinetic energy to evaporate. As the temperature increases, more water molecules will acquire enough kinetic energy to enter the vapor phase, thereby increasing the rate of evaporation.

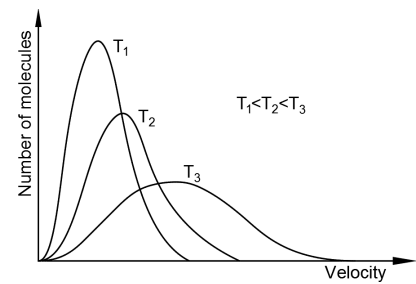


Figure 2.8: General velocity distribution of molecules for different temperatures.

With this in mind, consider a situation where water in an enclosed area evaporates at a constant temperature, that is, at a constant rate. As the amount of water vapor increases, the rate at which it condenses back into liquid increases as well since it becomes more likely for the molecules to hit the water surface and transition back into liquid. Eventually, the rate of condensation becomes equal to the rate of evaporation, assuming of course that there is enough water available for the rate of condensation to “catch up”. At this point the concentration of water vapor in the air remains constant and is said to have reached the so called dew point, meaning that it contains the maximum amount of water vapor possible for this particular temperature. This point corresponds to a relative humidity of 100 %. Thus, relative humidity gives a direct indication of how close the concentration of water vapor is to the dew point. In other words, where the water vapor concentration is on the range of possible water vapor concentrations for a certain temperature. For a higher temperature, the amount of water vapor needed to reach the dew point will be higher since the rate of condensation then needs to increase by a larger amount for it to become equal to the new higher rate of evaporation.

The humidity in a closed space can be controlled to a fixed value in a relatively inexpensive and simple way by adding a container of water saturated with a certain type of salt. The addition of the salt reduces the number of water molecules per unit volume since parts the volume is occupied by the dissolved salt. As a consequence, the number of water molecules on the surface decreases, see figure 2.9. Therefore, since evaporation occurs on the surface of a liquid, the rate of evaporation is reduced compared to the case with pure water. The rate of condensation, however, remains unaltered since the liquid surface area is the same. The reduced rate of evaporation results in a lower water vapor concentration at equilibrium than what it would be for a pure water surface, and hence, the relative humidity will be lower than 100 %. If another type of salt with a different solubility is used, the relative humidity at equilibrium

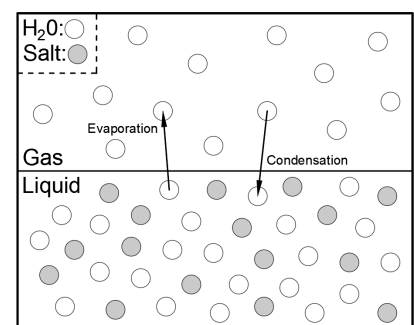


Figure 2.9: Closed system with a saturated salt solution.

changes accordingly. Thus, the humidity can be controlled by selecting an appropriate salt that gives the desired relative humidity. A collection of different solutes for controlling relative humidity from 3 to 98 percent can be found in [14].

2.4 Surface charge accumulation

Charge accumulation can occur at the interface between different materials in the presence of an electric field. To understand this phenomena in a macroscopic sense, consider two different dielectric (non-conductive) materials stacked on top of each other between two parallel plate electrodes, forming a so called Maxwell-Wagner capacitor (figure 2.10). If a positive DC voltage is applied to the top electrode while the bottom one is kept grounded, an electric field directed from the top plate to the bottom plate appears. This electric field does two things. First, it initiates extremely small conduction currents in the materials due to the non-zero conductivity present in non-ideal dielectrics. Second, it creates electric dipoles in the materials due to the polarization of bound charges, that is, the displacement of positive and negative charges in opposite direction. More specifically, a deformation of the negative electron cloud relative to the positive nucleus. The degree to which a dielectric material becomes polarized in response to an electric field is dictated by its relative permittivity ϵ_r . For the same applied electric field, a material with a high relative permittivity will have a greater separation of charges of different polarity than a material with a low relative permittivity.

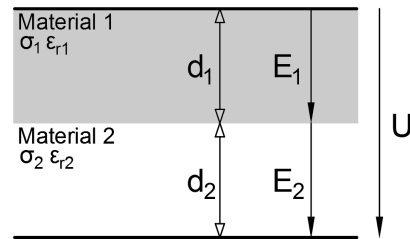


Figure 2.10: Maxwell-Wagner capacitor stressed with a constant DC voltage.

This is illustrated in figure 2.11 where it is assumed that material 2 has a higher relative permittivity than material 1 ($\epsilon_{r2} > \epsilon_{r1}$). The effect of this polarization is that it alters the electric field in the materials. In the bulk of the materials, each displaced charge has a neighbouring charge of opposite polarity and equal magnitude, and can therefore be seen as macroscopically neutral. At the surface boundary between the two materials, however, complete neutralization does not take place since the neighbouring dipoles are not polarized to the same degree. Because material 2 in this case has the highest permittivity, the negative charges overwhelm positive ones, resulting in a net negative charge. As the electric field from this charge is superimposed onto the initially applied background field, the field in material 1 is enhanced while the field in material 2 is reduced. Hence, a higher polarization in material 2 increases the conduction current in material 1 and reduces it in material 2, and vice versa.

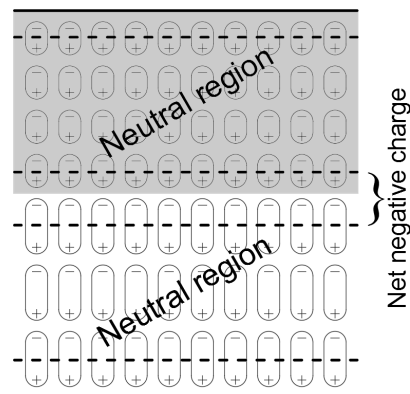


Figure 2.11: Polarization of the Maxwell-Wagner capacitor.

If it is also assumed that material 1 is the one with the highest conductivity ($\sigma_1 > \sigma_2$), it follows that it also has the highest current, since not only is the conductivity there higher but also the electric field due to polarization. The current in material 1 that approaches the material inter-

face is then positive since the direction of the electric field there is towards the boundary. As positive charge carriers reach the surface boundary they start to accumulate. The reason for this is that the other—less conductive—material is acting as a bottleneck. In other words, the rate at which charges enter the boundary is higher than the rate at which they leave it. Consequently, the electric field from these surface charges reduces the current in material 1 while increasing it material 2. Eventually, when enough charge has accumulated at the boundary, the currents in both materials are equal. At this point, the rate at which charges enter the boundary is equal to the rate at which they leave it, and hence no more charge accumulates. That is to say, the surface has become saturated. This process of surface charge accumulation is illustrated in figure 2.12.

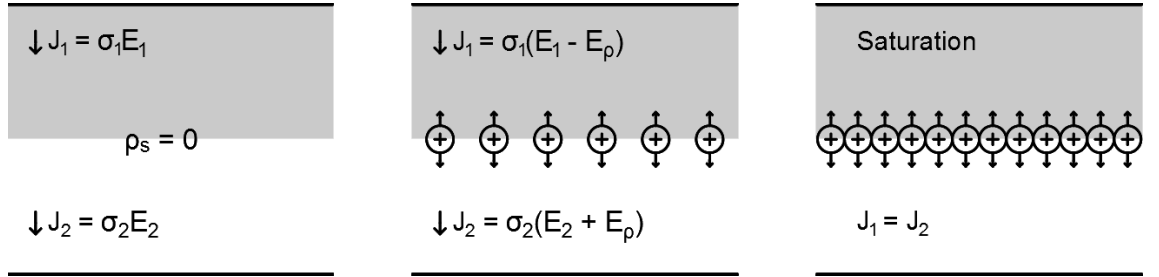


Figure 2.12: Surface charge accumulation process. (left) Initial positive currents as voltage is applied. (middle) Currents are affected by the field from surface charges. (right) Surface has reached saturation, the currents are equal.

Note that if the current in material 2 was the highest one instead, it would result in a net accumulation of negative surface charge. Therefore, from this simple example it can be concluded that the polarity of the surface charge is dictated by the polarity of highest initial current approaching the material interface. This can also be readily shown mathematically by, again, referring to figure 2.10. At steady-state, the currents in both materials are equal, hence

$$J = \sigma_1 E_1 = \sigma_2 E_2. \quad (2.12)$$

Furthermore, the total applied voltage is equal to the sum of the individual voltage drop over the materials

$$U = E_1 d_1 + E_2 d_2 \quad (2.13)$$

From these two equations, the electric field in the materials can be solved for as

$$\left. \begin{array}{l} J = \sigma_1 E_1 = \sigma_2 E_2 \\ U = E_1 d_1 + E_2 d_2 \end{array} \right\} \rightarrow E_1 = \frac{\sigma_2 U}{\sigma_2 d_1 + \sigma_1 d_2}, \quad E_2 = \frac{\sigma_1 U}{\sigma_2 d_1 + \sigma_1 d_2}. \quad (2.14)$$

Now, by applying the boundary condition for the electric displacement field \vec{D} an expression for the surface charge density ρ_s can be achieved.

$$\hat{n}_2 \cdot (\vec{D}_1 - \vec{D}_2) = \rho_s \quad (2.15)$$

Here, \hat{n}_2 is the outward unit normal from material 2 and depends on how the coordinate system is defined. If it is defined as in figure 2.13 equation 2.15 becomes

$$\hat{y} \cdot (-\hat{y}D_1 - (-\hat{y})D_2) = D_{2n} - D_{1n} = \rho_s, \quad (2.16)$$

which states that the normal component of \vec{D} is discontinuous across a surface where the discontinuity is equal to the surface charge density. The electric displacement field is related to the electric field through the constitutive relation $\vec{D} = \epsilon\vec{E} = \epsilon_0\epsilon_r\vec{E}$, where the constant ϵ_0 represent the permittivity in a vacuum. Applying this relation to equation 2.16 while inserting the expressions for the electric fields derived in 2.14 and solving for the surface charge density yields

$$\rho_s = \epsilon_0 U \frac{\sigma_1\epsilon_{r2} - \sigma_2\epsilon_{r1}}{\sigma_2d_1 + \sigma_1d_2} \quad [\text{C/m}^2]. \quad (2.17)$$

From this expression it can be seen that the polarity depends on which of the terms $\sigma_1\epsilon_{r2}$ and $\sigma_2\epsilon_{r1}$ in the nominator is the biggest. For example, by assuming a positive applied voltage U and $\sigma_1\epsilon_{r2} > \sigma_2\epsilon_{r1}$, the initial current in material 1 is the highest and will therefore result in a positive polarity of ρ_s , which is in agreement with the previous discussion.

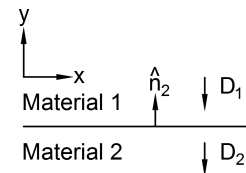


Figure 2.13:
Coordinate system definition.

2.5 Surface charge decay

Once electric charges are deposited on a surface they start to decay through various mechanisms. One of these mechanisms is the neutralization of charges through the bulk of the solid material (bulk neutralization), which is primarily due to intrinsic conduction [15]. As such, the rate of this type of decay is dictated by the bulk conductivity and is therefore generally extremely low for polymeric materials.

Another way surface charges can decay is by spreading along the surface towards a grounded point. This occurs if the charges are distributed unevenly as charges in regions of high concentration tend to spread (diffuse) into regions of lower concentration due to resulting tangential field. This decay process therefore depends on the charge distribution as well as the surface conductivity—which is strongly influenced by humidity [16]. Note, however, that this process does not necessarily cause a reduction of the amount of charges on the surface unless they manage to spread towards the ground, thereby forming a conductive channel.

If the charged surface is exposed to the surrounding air—or any other gaseous medium—yet another mechanisms contribute to the charge decay, namely, gas neutralization. Surface charges are then neutralized by free ions present in the gas which are attracted to the charged surface. This mechanism therefore depends on the amount of free ions in the gas as well as the potential of the surface since a higher potential attracts more ions. The three different decay mechanisms mentioned here are illustrated in figure 2.14.

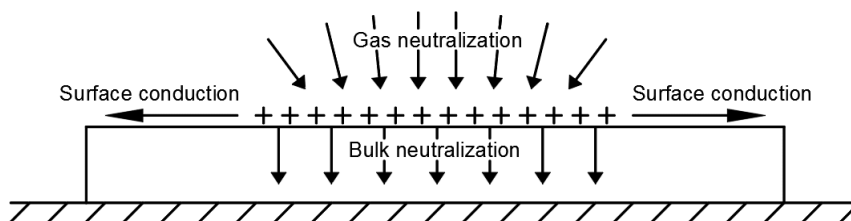


Figure 2.14: Surface charge decay mechanisms.

2.6 Field-nullifying method for non-contact surface potential measurements

The amount of charge deposited on a surface can be determined indirectly by measuring the resulting electric potential on the surface, that is, the surface potential. One widely used method for measuring surface potential is to use a capacitive probe as it allows for a non-destructive examination of the surface due to its non-contact nature [17]. As the probe is positioned above the charged surface, a parallel-plate capacitor is formed whose capacitance depends on the covered surface area A , the gap distance D and the permittivity of the insulating medium as

$$C = \varepsilon_0 \varepsilon_r \frac{A}{D} \quad [\text{F}]. \quad (2.18)$$

If U_1 and U_2 are the potentials—with respect to ground—on the probe and the surface respectively, then the voltage U over the capacitor can be expressed as $U = |U_1 - U_2|$, see figure 2.15. Whenever there is a discrepancy between U_1 and U_2 the voltage U becomes non-zero meaning that there exists an electric field across the gap. This field then causes a current to flow either to or from the probe depending on which potential is the highest. The prerequisite for the initiation of this current can be fulfilled if the gap distance changes. From equation 2.18 it can be seen that a change in the gap distance causes the capacitance to change accordingly. Since capacitance is a measure of the amount of charge Q that an electrical system can hold per unit voltage and is therefore defined as

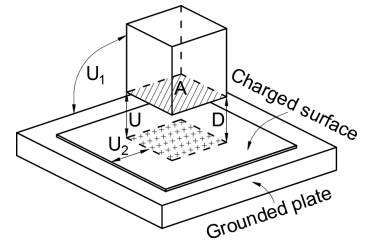


Figure 2.15: Capacitive probe above a charged surface forming a parallel capacitor.

$$C = \frac{Q}{U} \quad [\text{F}], \quad (2.19)$$

it follows that a change in capacitance results in a change in the voltage U (assuming that the charge is constant). The current through a capacitor is directly proportional to the rate of change of the voltage and is governed by the following equation

$$I = C \frac{dU}{dt} \quad [\text{A}]. \quad (2.20)$$

Therefore, whenever the gap distance changes, a current starts to flow through the capacitor. Another way a current can be initiated is if the charge on the surface changes. Again, according to equation 2.19 a change in charge Q must result in a change in voltage U if the capacitance is constant, which in turn makes the current non-zero. Since capacitance is entirely defined by geometry and material properties—which is in this case unaltered—it is indeed constant.

A common way to measure surface potential using a capacitive probe is to apply an external adjustable voltage to the probe. The potential difference U can then be brought to zero by making U_1 equal to U_2 . In other words, enforcing the potential on the probe to be equal to the potential on the investigated surface. As a consequence, any electric field across the gap is nullified along

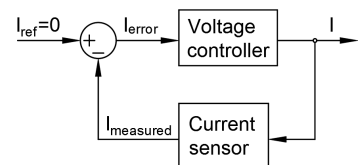


Figure 2.16: Feedback control loop.

with the corresponding current. Hence, this method is referred to as field nullifying, or the null method. From the previous discussion it has been demonstrated that a current is initiated while measuring if the gap distance or the surface charge changes, meaning that $U_1 \neq U_2$. To ensure that the electric field is nullified at all times, the current must be continuously measured and fed into a feedback control loop which regulates the applied voltage in such a way that the current becomes zero. The principle of this is illustrated schematically in figure 2.16.

Once the surface potential is measured, the corresponding surface charge density can be determined through electrostatic field calculations. For this purpose, the boundary condition for the electric displacement field (equation 2.15) can be used yet again. By considering the same coordinate system definition as in figure 2.13 as well as a uniform charge distribution, the situation can be represented as in figure 2.17. Due to field nullification, the electric field in medium 1 right below the probe is zero. In medium 2, however, it is simply equal to the surface potential V divided by the material thickness d because of the assumed uniform charge density ρ_s producing a uniform field. The expression for converting between surface potential to surface charge density then becomes

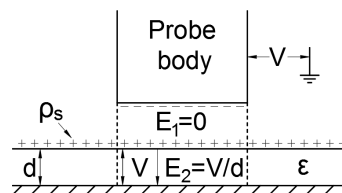


Figure 2.17: Electric field beneath the probe while measuring surface potential for a uniform charge density.

$$\rho_s = \epsilon \frac{V}{d} \quad [\text{C/m}^2]. \quad (2.21)$$

Bear in mind that if the surface is charged non-uniformly, the local charge distribution beneath the probe still appears quite uniform as it only measures a very small portion of the surface. Think of it as zooming into the boundary of a circle, the greater the zoom the less pronounced the curvature becomes and the flatter the boundary appears. Although, if the surface is charged extremely non-uniformly, equation 2.21 is no longer accurate and would therefore introduce an error. Nonetheless, this error can be minimized by ensuring that the probe is positioned as close to the surface as practically possible, thereby increasing its resolution.

2.7 Ion emission from water adsorbed onto metal surfaces under high electric fields

Water (H_2O) is composed of two hydrogen atoms covalently bonded to an oxygen atom. The oxygen atom has six electrons in its outer shell (valence electrons) whereas the hydrogen atoms only have one. This means that in the water molecule, the oxygen atom gets access to all eight electrons required to fill its outer shell—four of its own electrons and two electron pairs which it shares with the hydrogen atoms. It is therefore surrounded by a total of four electron pairs which form electron clouds directed towards the corners of a tetrahedron. The two non-binding electron pairs exert a force on the binding electron pairs which pushes them together, resulting in a binding angle of 104.5° . As such, water is an angled molecule, see figure 2.18. Due to the fact that oxygen has a high electronegativity value compared to hydrogen (3.5 for oxygen and 2.1 for hydrogen) the binding electrons are drawn towards the oxygen atom quite strongly. Because of

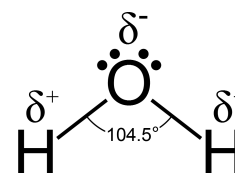


Figure 2.18: Structural formula of water.

water's non-linear structure, the center of the positive charge does not coincide with the center of the negative charge. Hence, water is a polar molecule with two poles, that is, a dipole where the oxygen atom has a slight excess of negative charge δ^- and each hydrogen atom has a slight excess of positive charge δ^+ [18].

The polarization of water results in an attractive force between oxygen and hydrogen of different water molecules. This weak intermolecular force is known as a hydrogen bond and is illustrated in figure 2.19. Hydrogen bonding between water molecules leads to the formation of a range of different water clusters, that is to say, discrete hydrogen bonded assemblies of water molecules. These hydrogen bonds are continually breaking and reforming due to thermal motion. A water cluster can be denoted as $H_2O_{(n)}$ where n indicates the amount of molecules within the cluster. Another consequence of the polar nature of water is that it results in self-ionization. As water molecules randomly move around they occasionally orient themselves in such a way that they produce an electric field—due to their dipole moment—which is strong enough to break a covalent bond between oxygen and hydrogen [19]. The resulting dissociated water molecule then becomes a hydroxide (OH^-) as it releases one of its hydrogen atoms, which in turn rapidly attaches to a nearby water molecule forming hydronium (H_3O^+). This process also happens in reverse when an hydroxide and hydronium meet; they then recombine forming two individual water molecules. As such, the self-ionization of water can be express with the following equilibrium reaction

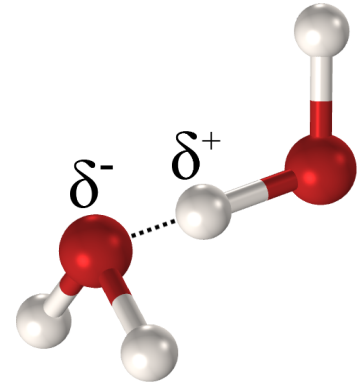
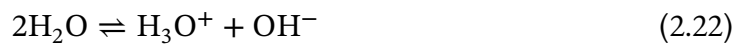


Figure 2.19: Schematic showing a hydrogen bond.



where the amount of water ions at equilibrium depends on the temperature [20]. This is what gives water its conductive properties as it always contains a certain amount of ions which can act as charge carriers.

It turns out that water vapor can adsorb onto surfaces of crystalline materials such a metals via weak van der Waals forces [21]. This in turn can lead to the growth of water clusters at the metal interface where the amount of adsorbed water (or the size of the clusters) depends on the relative humidity. According to [21], water adsorbed on crystalline materials generally exhibits an exponential increase with relative humidity. If the metal is energized with a high voltage, the resulting surface electric field is believed to initiate the following electrochemical reaction that dissociates the adsorbed water clusters into water cluster ions [5]



For this to happen there needs to be a high local concentration of adsorbed water to provid an environment for self-ionization. As water ions are generated they experience a force from the applied electric field and begin to drift accordingly. For a positive applied voltage, the hydroxide (OH^-) moves towards the energized metal while the hydron (H^+) moves in the opposite direction. As the hydron begins to pull away, it attracts oxygen atoms of nearby water molecules, resulting in the emission of a protonated water cluster $H^+(H_2O)_m$. Hence, water adsorbed on

electrode surfaces can act as a source of charge carriers, thereby increasing the apparent conductivity of air. This rather simplified explanation of the mechanism for the field emission of water ion clusters is illustrated in figure 2.20.

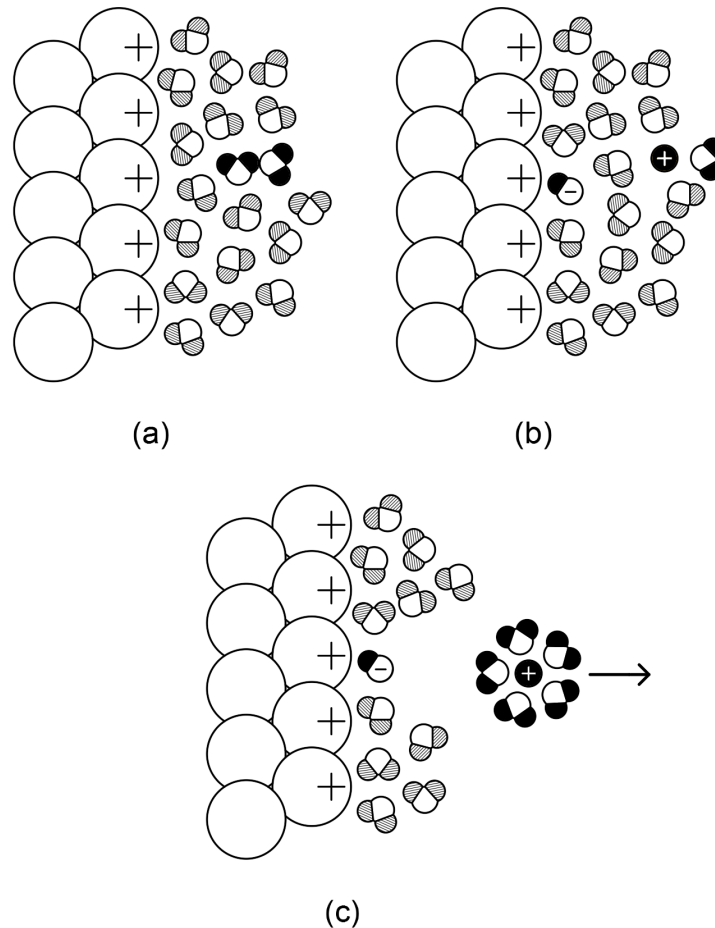


Figure 2.20: Mechanism for a positive field emission of water ion clusters. (a) Water adsorbed onto energized metal begins to self-ionize. (b) After self-ionization, the hydroxide moves towards the metal surface while the hydron moves towards the gaseous interface for emission. (c) The hydron pulls the oxygen of nearby water molecules towards it and a protonated water ion cluster is released.

In [22], water ion cluster formation on a platinum electrode was determined for different electric field strengths. It was found that as the field strength increased, protonated water ion clusters $H^+(H_2O)_n$ were emitted and the ion emission onset field turned out to be lower for larger clusters. This result is in accordance with the MSc thesis work by P. Mundim [4] where the current between two parallel plate electrode in air was measured for different levels of humidity. As previously stated, it was found that the current exhibited an exponential increase with relative humidity. This makes sense since in [21] it was shown that the amount of adsorbed water generally increases exponentially with the relative humidity as well. Thus, a higher relative humidity leads to larger cluster formations which in turn are emitted more easily, thereby resulting in a larger current. With this in mind, it certainly seems that ions released from adsorbed water due to an applied electric field is indeed an established phenomena.

3 Method

This chapter focuses on the methods used for accomplishing the thesis objectives. It begins with a review of the developed experimental setup. Following this comes an explanation of the procedure used for surface charging and surface potential measurements. Lastly, it covers how the impact ionization voltage (electron avalanche onset voltage) is approximated by calculating the maximum electric field as a function of the applied voltage using Comsol Multiphysics.

3.1 Experimental setup

An overview of the experimental setup is shown in figure 3.1. As can be seen, the part of the setup where surface charging and surface potential measurements take place is contained within a sealed plastic box—functioning as a humidity chamber. The bottom of the box is fitted with a grounded copper sheet on top of which lies a thick copper plate where the (90 mm x 90 mm x 0.5 mm) teflon sample is attached using double adhesive aluminium tape. This is to ensure that the sample is properly connected to ground but also so that it can easily be moved around as needed. The sample has an electrical conductivity $> 10^{-20}$ S/m [23], which is indeed lower than the conductivity of air ($\sim 10^{-15}$ to $\sim 10^{-9}$ S/m) [24]. This makes it so that surface charges originate from the surrounding air and not from the sample itself since $\sigma_{air}\epsilon_{sample} > \sigma_{sample}\epsilon_{air}$, see equation 2.17. This is preferable since air is the medium where a humidity dependence of the current is expected.



Figure 3.1: General view of the experimental setup.

A plastic pipe attached to a linear positioning system is passed through the box, allowing it to move back and forth along its axis. Mounted on the pipe is a capacitive probe which is held in place using ordinary duct tape and is mechanically supported by a piece of wood, see figure 3.2. It utilizes a field-nullifying method for surface potential measurements and is connected to an electrostatic voltmeter equipped with a data acquisition card to send signals from the probe to a computer. Below the probe is yet another piece of copper with the same thickness as the copper plate that holds the sample. It is used during calibration to make sure that the voltmeter reads zero volt when the probe is a certain distance above ground. Also in the box are two plastic containers with a saturated salt solution to regulate the humidity along with a hygrometer to monitor and measure relative humidity. To prevent water vapor from leaking out of the box, the ends of the pipe are taped shut and the brim of the various holes made in the box are taped as well.

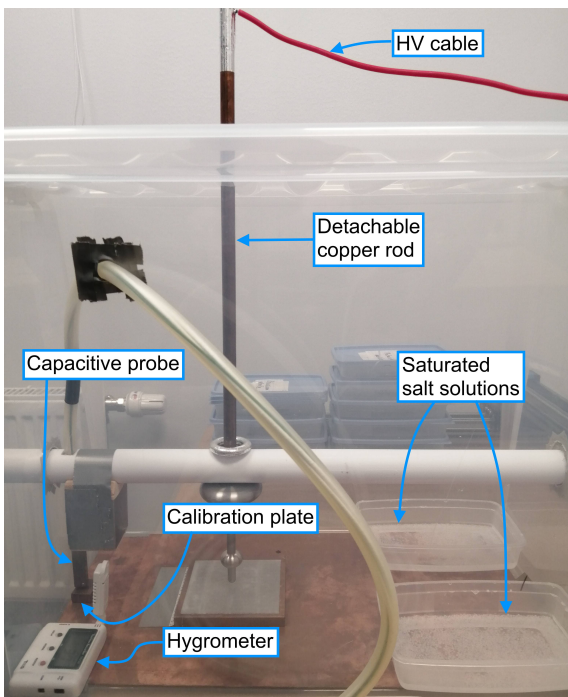


Figure 3.2: Detailed view of the humidity chamber.

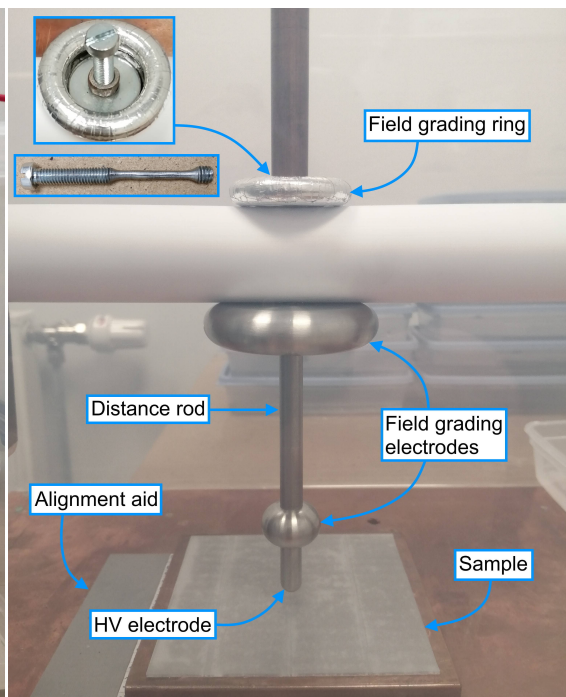


Figure 3.3: Detailed view of the electrode arrangement.

Also mounted on the pipe is an electrode arrangement attached to a screw which in turn is secured to the pipe with a nut, see figure 3.3. In order to energize the arrangement, a long copper rod connected to an HVDC generator of either positive or negative polarity is placed over the screw and nut. The reason for energizing in this manner is to cover sharp edges of the screw's threads but also to achieve a symmetrical field distribution above the pipe with respect to the sample. Due to the fact that charge tends to concentrate at points on charged conductors where the curvature is particularly high—and as such could give rise to unwanted high electric fields—it motivates one to avoid or cover up such points. In this case, the largest electric field should appear at the tip of the electrode where its distribution and magnitude easily can be predicted to achieve a controlled charging of the sample. Consequently, geometric field grading is here used to cover up any screw threads and sharp joints in the electrode setup—prevent them from acting

as potential sources of charge. That being said, the electrode configuration consists of a rod electrode with a radius of 4 mm attached to a distance rod via a small field grading electrode. This rod is then secured to yet another larger field grading electrode connected to the screw through the pipe. Note that the part of the screw that is inside the pipe has had its threads removed as these would not be shielded by the pipe since it is not a conductor, again see figure 3.3. Also, to reduce the electric field from the edge of the copper rod, a field grading ring made out of wood wrapped in aluminum tape is used. Altogether, this arrangement results in a distance of 3 mm between the rod electrode and the sample. It can, however, be reduced by inserting conducting plates underneath the copper plate to raise the sample if needed.

3.2 Experimental procedure

Prior to charging, the sample is cleaned with isopropanol and left to air dry. The isopropanol binds to static charge on the surface, thereby neutralizing it as the isopropanol evaporates which occurs rather rapidly [25]. Thereafter, the surface potential on the sample is measured to ensure that the sample is properly neutralized. This is done by moving the pipe using the linear positioning system so that the probe is swept across the sample—roughly 1 mm above it—at a constant speed. Before this, however, the probe is first manually calibrated by adjusting an offset voltage on the voltmeter until it reads zero volt as the probe is above the calibration plate. Bear in mind that there will be about ± 10 V of signal noise for a completely neutralized sample. Next step is to put the lid on the box, place the copper rod on top of the electrode arrangement and wait for the relative humidity to reach an equilibrium steady state. This take a few hours depending on which type of salt solutions is used, see figure 3.4. Note that these values differ a bit from the ones in [14], which is probably due to the box not being fully sealed and the temperature varying ever so slightly. Even so, as long as the relative humidity consistently settles at a value somewhat close to what is expected it is good enough.

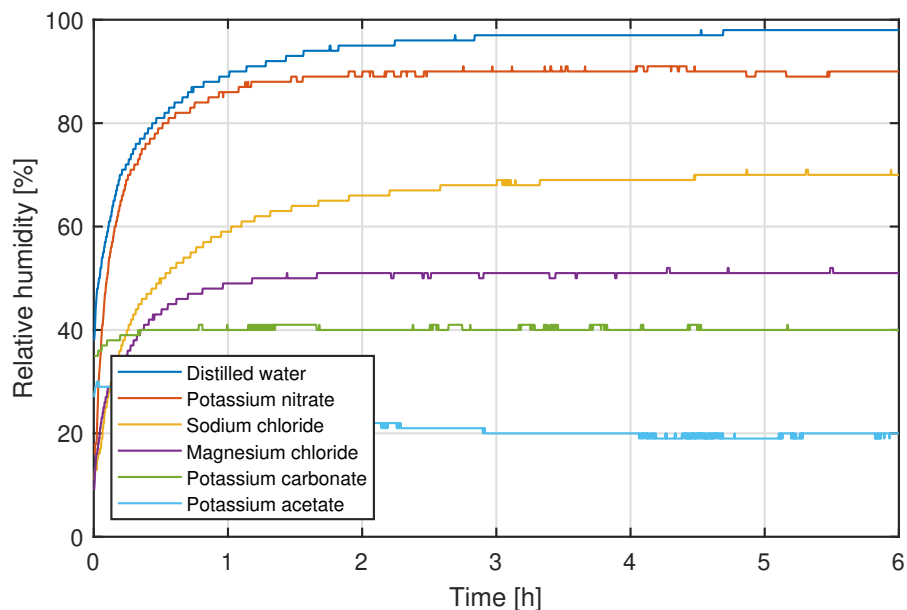


Figure 3.4: Relative humidity response for different saturated salt solutions at 20°C.

Once equilibrium is reached, the surface charging is initiated by turning on the HVDC generator to energize the electrode. When the charging is deemed to be finished, the electrode is de-energized and the copper rod is removed. After that, the surface potential is measured either along a single line through the sample's center or along multiple ones—37 to be specific—spanning the whole surface to achieve three-dimensional perception of the surface charge distribution. The latter is done by manually shifting the sample between measurements using a piece of squared paper taped onto the copper sheet as an alignment aid.

3.3 Simulation of electrostatic field in Comsol Multiphysics

Comsol Multiphysics is a software that numerically solves partial differential equations from various branches of physics for a given geometry, material properties and initial conditions. It is generally used if the problem in question is too complex or time-consuming to solve analytically with pen and paper. It does this by utilizing the finite element method which, simply put, divides an objects complex geometry into smaller simpler parts (finite elements) which together forms a so-called mesh. The resulting simple equations that apply to these finite elements are then solved and assembled back into a larger system of equation that model the whole object. Lastly, a solution is approximated by minimizing an associated error function achieved using various variational methods. The denser the mesh, that is, the more the geometry is divided into smaller parts, the more accurate is the final solution. A finer mesh, however, leads to a greater computation time meaning that there is a trade-off between accuracy and the time required to find a solution.

To find out which voltage levels results in local development of electron avalanches, knowledge about the maximum electric field is needed as a function of applied voltage. The voltage corresponding to a maximum electric field of around 2.5 kV/mm is then approximately the onset voltage for electron avalanches according to previous experiments [13]. In this case, the maximum electric field appears right as the electrode is energized—before any surface charge has had time to accumulate. This is because the electric field due to surface charge would cancel out part of the electric field from the electrode, resulting in an overall lower field strength. This therefore boils down to an electrostatic problem as that would yield the the electric field at the instant of energization. Accordingly, the electrode arrangement is here modeled in Comsol to determine its electrostatic field distribution for different voltage levels.

3.3.1 Electrostatics - governing equations

The mathematical model of electrostatics in free space is composed of the following two equations that specify the divergence and curl of the electric field

$$\nabla \cdot \vec{E} = \frac{\rho_v}{\epsilon_0} \quad [\text{V/m}^2], \quad (3.1)$$

$$\nabla \times \vec{E} = 0. \quad (3.2)$$

Their validity has been unquestionably established by numerous experiments and are as such, fundamental postulates as they cannot be derived from any other equations. Equation 3.1 es-

establishes that a static electric field is non-solenoidal unless the volume charge density ρ_v is zero. In other words, it contains no sources or sinks without the presence of a volume charge density. It is also a form of Gauss's law which states that the total outward flux of the electric field over an arbitrary closed surface in free space is equal to the total charge Q enclosed by the surface divided by ϵ_0 . This can readily be shown by taking the volume integral of both sides and then applying the divergence theorem

$$\int_v \nabla \cdot \vec{E} dv = \frac{1}{\epsilon_0} \int_v \rho_v dv = \frac{Q}{\epsilon_0} \Rightarrow \underbrace{\left[\int_v \nabla \cdot \vec{A} dv = \oint_S \vec{A} \cdot d\vec{s} \right]}_{\text{divergence theorem}} \Rightarrow \oint_S \vec{E} \cdot d\vec{s} = \frac{Q}{\epsilon_0}. \quad (3.3)$$

Equation 3.2, on the other hand, simply asserts that a static electric field is irrotational, meaning that it has no net circulation. According to vector calculus, an irrotational field is also a conservative field and can therefore be represented as the gradient of a scalar field as

$$\vec{E} = -\nabla V \quad [\text{V/m}], \quad (3.4)$$

thereby defining the electrostatic potential V . Here, the minus sign is merely an old convention to express that the potential increases when going against the field. For equation 3.1 to also be valid in dielectric media and not just free space it needs to be modified to incorporate the effect of polarization. For this purpose, another field quantity is defined, namely, the electric displacement field \vec{D} as

$$\vec{D} = \epsilon_0 \epsilon_r \vec{E} = \epsilon \vec{E} \quad [\text{C/m}^2]. \quad (3.5)$$

Here, ϵ is again the permittivity of the medium and is a measure how much the bound charges in a material become polarized under the influence of an electric field. The vector \vec{D} thus encompasses both the electric field due to free charges as well due to the displacement of bound charges, hence the name electric *displacement* field. Going back to equation 3.1, the definition 3.5 now enables one to write a simple divergence relation between the electric field and the distribution of free charges in any medium as

$$\nabla \cdot \vec{D} = \rho_v \quad [\text{C/m}^3]. \quad (3.6)$$

Combining equations 3.4, 3.5 and 3.6 yields the following partial differential equation known as Poisson's equation

$$\left. \begin{array}{l} \vec{E} = -\nabla V \\ \vec{D} = \epsilon \vec{E} \\ \nabla \cdot \vec{D} = \rho_v \end{array} \right\} \rightarrow -\nabla \cdot (\epsilon \nabla V) = \rho_v \quad [\text{C/m}^3]. \quad (3.7)$$

This is the equation that is solved for in Comsol's electrostatic physics module for the given geometry, material and charge distribution to calculate the electrostatic potential and field.

3.3.2 Model implementation

When implementing the geometry of an object in Comsol it could be tempting at first to design a complete three-dimensional model. This, however, usually requires quite a lot of computational resources and could accordingly result in extremely long solving times. Therefore,

building a full 3D model ought to generally be avoided if possible. This is the case if the object to be modeled is symmetric in some way. The symmetry can then be utilized to greatly reduce the computational domain, resulting in faster solving times.

Considering the simple geometry of the electrode arrangement, it would in this case be rather straightforward to build and solve a full 3D model of it without any particularly long solving times. Even so, the fact that the electrode is symmetric around its axis is still considered here as it is deemed to be a more elegant design. Utilizing its rotational symmetry, it is sufficient to only consider a two-dimensional cross-section of half the model along its symmetry axis. The resulting computational domain of the model can be seen in figure 3.5 which consists of two material domains; air and teflon. Note that only the surface boundary of the electrode is modeled since the electrostatic field inside an energized conductor is always zero, and is therefore not necessary to calculate. To implement equation 3.7 as the partial differential equation to be solved, the physics module electrostatic is used. Next, conditions for the four different boundaries need to be specified. Electric potential is applied to the electrode boundary while zero charge condition is applied to the two open boundaries as per default. Lastly, zero potential (ground) is applied to the ground boundary. Regarding the material properties, only relative permittivity is required to be specified in electrostatics, which is about 1 for air and 2.1 for teflon.

Figure 3.6 illustrates the generated mesh of the domain. For simplicity, a triangular mesh is used as it can easily divide a complex geometry into smaller parts without distorting its original shape —provided that enough detail is given at high curvature regions. Since an accurate representation of the maximum electric field is of interest, the mesh is refined around the tip of the electrode—locally increasing the accuracy of the solution. This refinement is clarified in the large red rectangle in figure 3.6 which provides a zoomed in view of the area around the electrode tip.

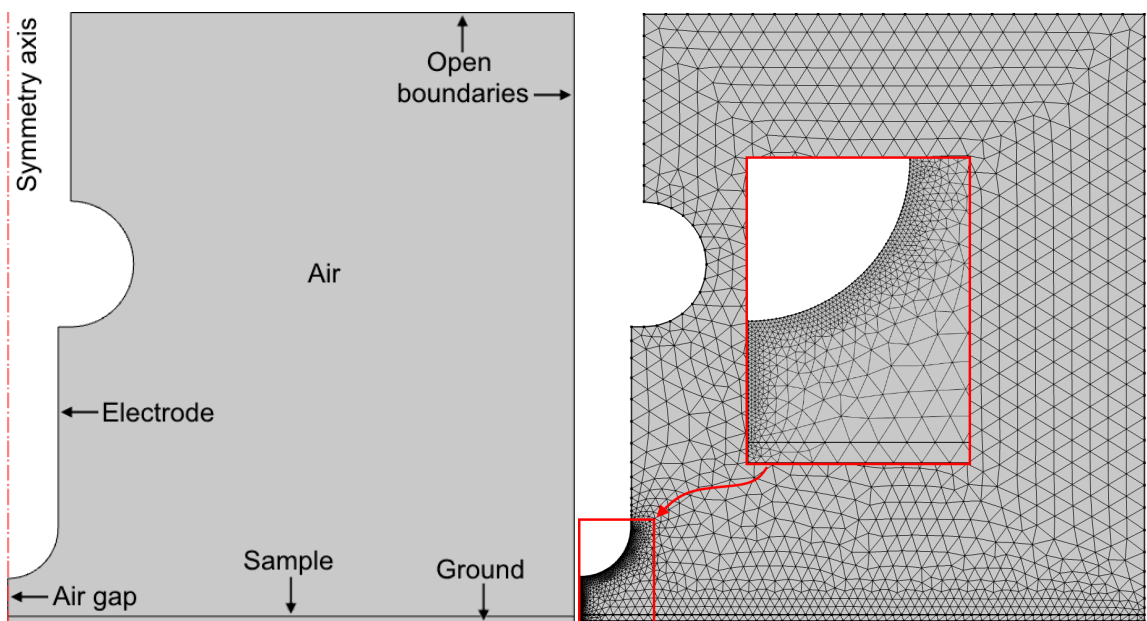


Figure 3.5: Geometry of the computational domain.

Figure 3.6: Illustration of the generated triangular mesh.

3.3.3 Solution

Poisson's equation is solved for the implemented model with its specified constraints using a stationary solver. In practice, this yields the electrostatic potential and field right as the voltage is applied. That is to say, the capacitive field distribution for which the electric field has its maximum value. Because the maximum electric field as a function of the applied voltage is of interest, a parametric sweep of the applied voltage is used while solving. The solution then contains the electric field distribution for multiple voltage levels. Figure 3.7 shows the electric field magnitude for the case that 4 kV is applied to the electrode. As can be seen, the maximum electric field occurs at the tip of the electrode where the distance to ground is the shortest and is around 2 kV/mm. Hence, the electric field is evaluated at that point for different voltage levels. Also worth noting is that the electric field inside the sample is very low. This is simply because it has a higher relative permittivity than air and is therefore more polarized. In fact, air cannot be polarized at all since it has no bound charges which is why its relative permittivity is unity. The polarization taking place in the sample results in an internal electric field to be generated which cancels out a portion of the external electric field.

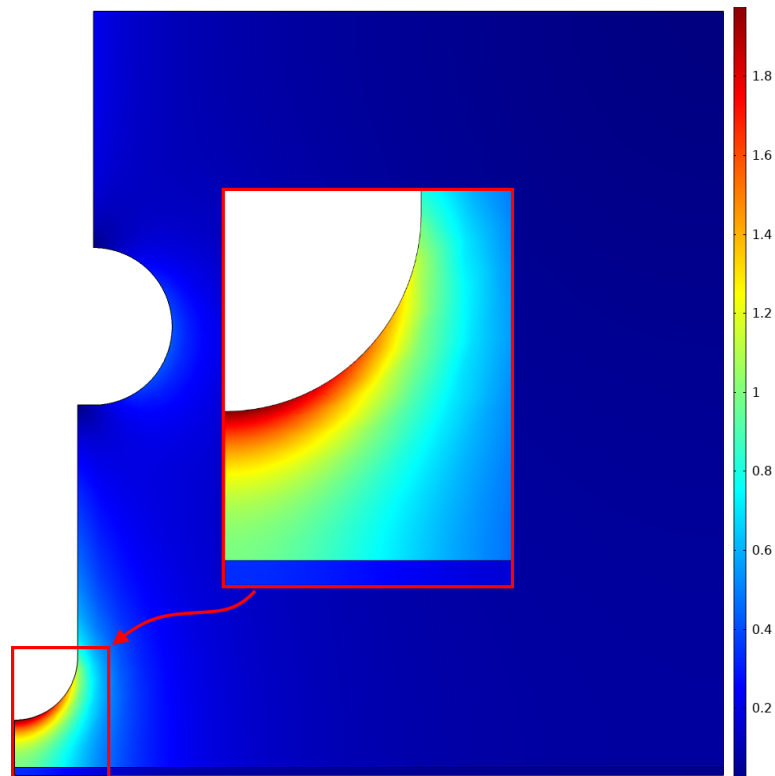


Figure 3.7: Electric field magnitude as the electrode is energized with 4 kV.

The maximum electric field as a function of the applied voltage is plotted in figure 3.8. As one can observe, the voltage corresponding to a maximum electric field of 2.5 kV/mm is found to be 5 kV and is therefore approximately the onset voltage for electron avalanches. Anything above this value results avalanche development around the electrode tip and should therefore be avoided. To be on the safe side, however, a voltage of 4 kV is used throughout the measurements leaving a margin of 0.5 kV/mm. That way, the electric field in the air gap is low enough to

prevent ionization by collision. In other words, it is within the saturation region, although there could be a part of the gap that is within the ohmic region as the threshold between these two is not known. Even so, it can be ensured that—at least in theory—any contribution of charges from adsorbed water clusters will not be “drowned out” by more dominant electron avalanches.

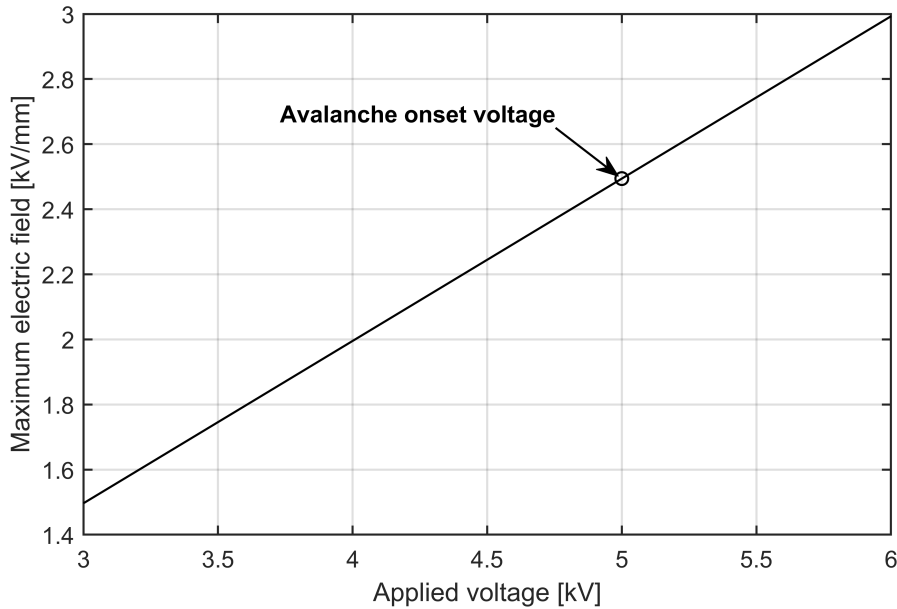


Figure 3.8: Estimated avalanche onset voltage for the modeled electrode configuration.

Also, note the linear dependence between the electric field and the applied voltage. This makes sense since the magnitude of the electric field is equal to the derivative of the voltage (equation 3.4). So, if the voltage on the rod electrode increases by a certain factor so does its derivative across the air gap since the voltage on the copper plate remains unaltered. Putting it differently, the spatial rate of change of the voltage between the two electrodes goes up by the same factor as the voltage applied to the rod. The slope, on the other hand, is dictated by the geometry which here is the gap distance and the electrode radius.

4 Results and discussion

In this chapter, the experimental results from the surface charging experiments are presented and discussed. More specifically, the measured surface potential of the flat teflon sample charged using both a positive and negative voltage under different humidity levels. In addition to this, the raw data is processed to determine the corresponding charging dynamics as well as the initial charging rate. A discussion regarding the charge distribution is also provided based on the interpolation between multiple measurements spanning the entire sample. All measurements presented here are conducted at a temperature of approximately 20°C using a rod electrode with a radius of 4 mm, an air gap of 3 mm and an applied voltage of ± 4 kV.

4.1 Humidity dependence

The humidity dependence of surface charge accumulation is here visualized in three different ways. First, by comparing the developing charging patterns of the surface potential along a single line across the sample's center for various humidity levels. Second, by calculating and comparing the total line charge density over time, that is, the charging dynamics for different degrees of humidity. And lastly, by calculating the initial charging rate as a function of relative humidity. All this is of course done for both polarities—starting with negative.

4.1.1 Negative polarity

Presented in figure 4.1 is the surface potential of the negatively charged sample measured along a single line through its center at 15 minute intervals over a 4-hour period for various degrees of relative humidity. Not all measurements are shown here though as that would be too cluttered. Instead, a few carefully selected ones are shown to clearly illustrate the emerging charging patterns and allow for an easy comparison between different humidity levels. As can be seen, the polarity of the surface potential is the same as the applied voltage meaning that the net surface charge originate from that air, which is in agreement with equation 2.17. But more importantly, there is indeed a substantial humidity dependence of the surface potential—and therefore of the surface charge as well—increasing with relative humidity. Furthermore, no significant charging occurs at 40% relative humidity which is here the next lower humidity level. This means that the contribution of surface charge from natural ionization of air is in this case negligible and below the resolution of the present measurement method—at least for a 4-hour period. This is not that surprising since the average rate of charge carrier generation due to natural ionization is a mere 10 ion-pairs per cubic centimeter per second [8].

Another thing that can be observed is that initially—for low surface potential values—the charge growth is rather symmetric. But once the surface potential reaches a value somewhere between -1.5 and -1 kV it starts to become asymmetric. The reason for this could be due to a non-uniform surface conductivity. As the surface potential increases, so does the the tangential component of the electric field from the surface charge, that is, the electric field whose direction is parallel to the surface.

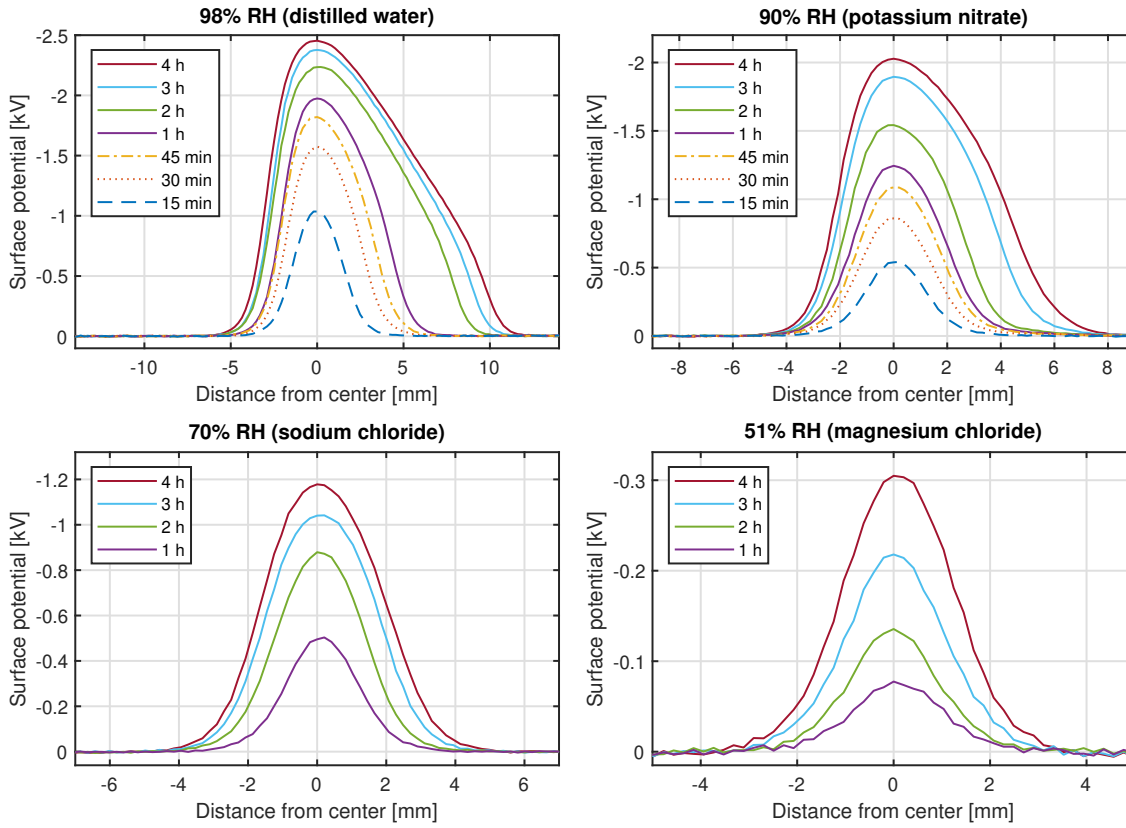


Figure 4.1: Measured surface potential of the negatively charged sample along a single line through its center at different time instances and relative humidity levels.

Since the charge distribution is non-uniform, a non-zero tangential component certainly exists. This tangential field then exerts a force on charges along the surface, causing them to spread from regions of high concentration into regions of low concentration, thereby initiating surface conduction. Eventually, surface conduction becomes substantial to the point where the non-uniformity of the surface conductivity becomes evident. Furthermore, since the surface conductivity is believed to increase with humidity, it could also play a role in increasing surface conduction. Why the surface conductivity would be non-uniform to begin with, however, is not clear. It could be that it is simply an intrinsic property of this particular sample. Another explanation is that there exist local variations of the electric field along the surface because of how the sample is attached to the grounded plate. The presence of any small air pockets between the sample and the ground definitely affects the surface electric field to some extent which could contribute to the non-symmetry of the surface conduction, but it is just a speculation.

In order to get a more clear picture of how much the charging is affected by humidity as well as how it changes over time, the raw data is processed as follows. First, the measured surface potential is converted into surface charge density using equation 2.17. This yields the same curve shapes as before but scaled down by a factor of $\epsilon/d = 3.72 \cdot 10^{-8}$. After that, the area under each surface charge density curve is calculated using trapezoidal integration. Since the surface charge density [C/m^2] is multiplied with dx during the integration—which here has the unit [m —each calculated area corresponds to a line charge density with the unit [C/m]. This represents the amount of charge per unit length along the direction perpendicular to the

line of integration—or the measured line—see figure 4.2.

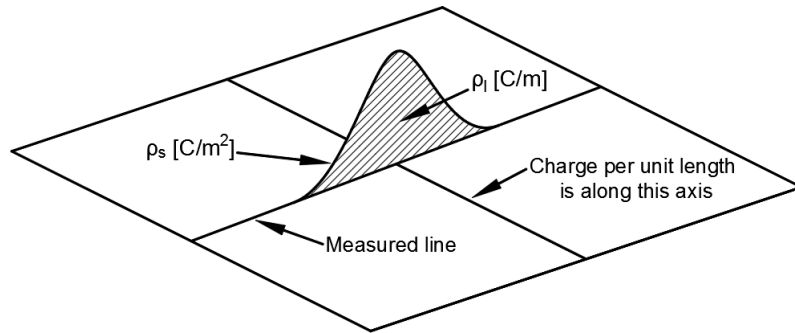


Figure 4.2: Clarification of the axis with a charge per unit length (line charge density).

The calculated line charge densities are plotted in figure 4.3 as a function of time along with fitted curves, clearly illustrating the humidity dependence of the charging dynamics. From the figure it can be seen that the line charge density increases linearly for the two lower humidity levels, indicating that the surface is far away from saturation. For the higher humidity levels, on the other hand, the charging rate decreases over time as the surface approaches saturation. Note the substantial increase when going from 90 to 98% RH—a mere eighth percentage points—implying that the relation between humidity and charging rate is extremely non-linear.

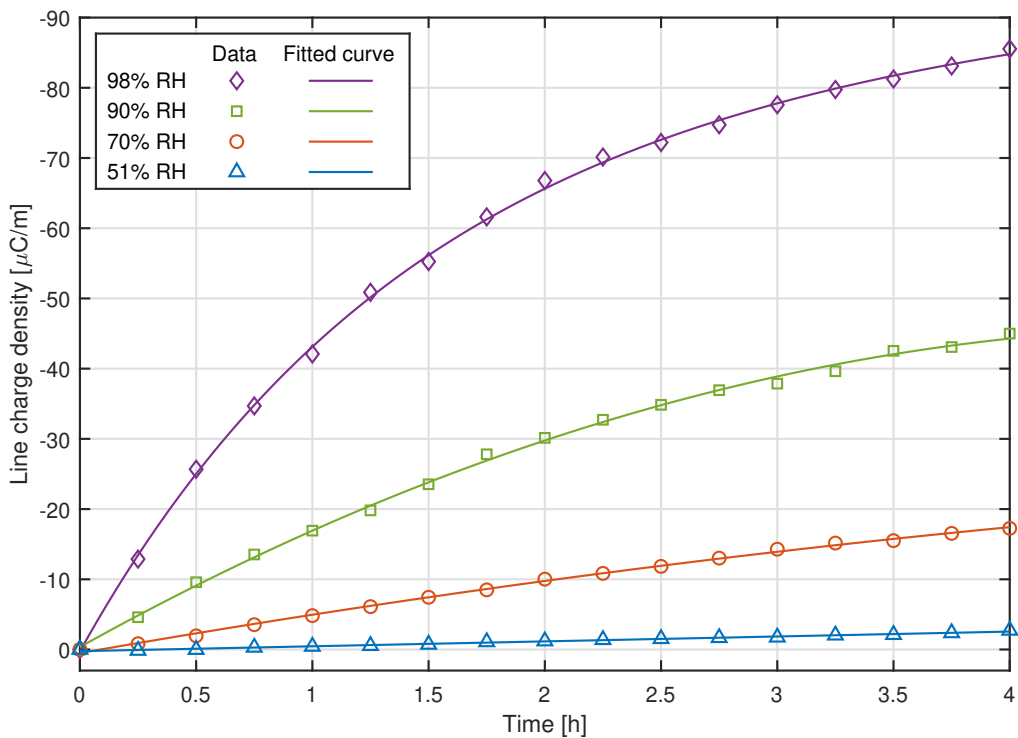


Figure 4.3: Negative charging dynamics for different humidity levels. Each data point is the result of an integration of the corresponding surface charge density curve.

For the purpose of finding the actual relation between humidity and charging rate, the *initial* slope is calculated for the different fitted curves. That way, the charging rate is not altered by the presence of any surface charge since at that time instant, no surface charge has had time to accumulate. When calculating the initial slope, the line charge density is divided by dt which has the unit [s]. As a consequence, the resulting unit becomes $[C/(sm)] = [A/m]$, that is, a *surface* current density. To understand this, imagine a surface perpendicular to the sample along the measured line, see figure 4.4. The current then flows from the tip of the electrode towards the sample along this surface. Presented in figure 4.5 are the calculated surface current densities—representing the initial charging rates—together with a curve fitted to the data as a function of relative humidity. As can be observed, the data points fit quite well to an exponential function of the form ae^{bx} where $a = -0.001412$ and $b = 0.09446$. This clearly shows that there is indeed an exponential dependence between the initial current and relative humidity, which is in agreement with what was found in [4].

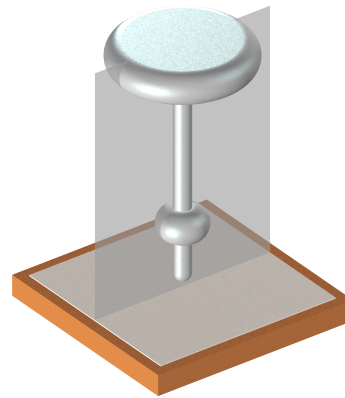


Figure 4.4: Hypothetical surface with a surface current density.

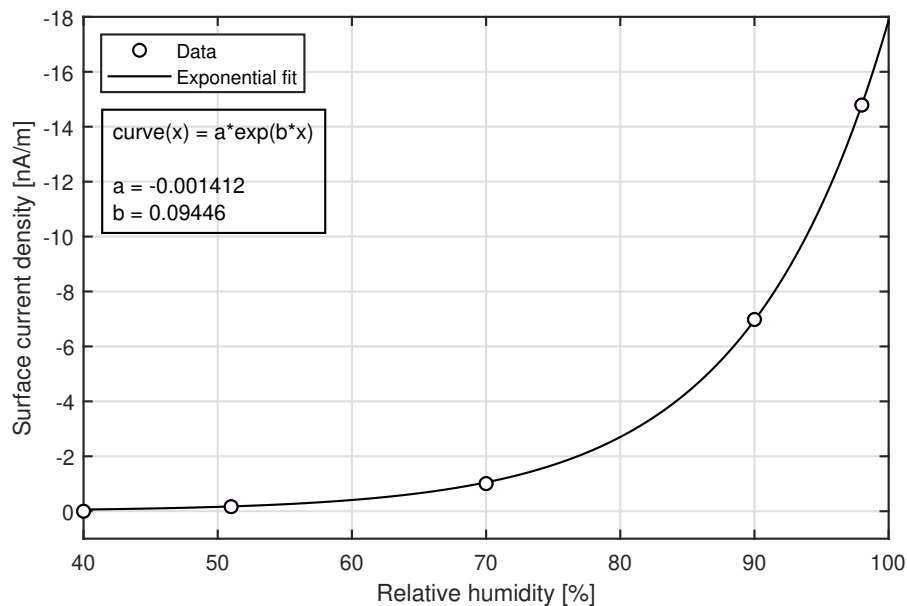


Figure 4.5: Initial charging rate as a function of relative humidity for a negative applied voltage. Each data point is the initial slope of the matching fitted curve in figure 4.3.

Furthermore, because the electric field in the air gap is operating within the saturation region—where the current is dictated by the rate of charge generation—it means that the observed current increase must be due to an increase in the rate of charge generation. As previously mentioned, however, there could be a part of the gap where the field is low enough to be within the ohmic region—where the current is dictated by the conductivity. Nonetheless, the current increase still has to be because of an increase of charge carriers. The other alternative would be if the mobility of the charge carriers increased. But this can not be the case because of what was mentioned at the end of section 2.1, namely that water vapor has a negative effect on charge

carrier mobility. Therefore, the result in figure 4.5 is proof that there exists a charge generation mechanism that is dictated by humidity. A final point to be made here is that the exponential characteristic could be inherited from the fact that the amount of adsorbed water vapor also exhibit an increasing exponential dependence with humidity [21]. If such is the case, it is an indication that this charge generation mechanism is a surface phenomena, and is therefore in agreement with the simplified charge generation mechanism mentioned in 2.7.

4.1.2 Positive polarity

For the purpose of investigating whether the humidity dependent charge generation mechanism also depends on the polarity of the applied voltage, the same analysis is here done for a positive polarity. Figure 4.6 shows the developing charging patterns for a positively charged sample. To be specific, a selection of the surface potentials measured at different moisture levels along a straight line through the sample's center at 15 minute intervals over a 4 hour period. The first thing that stands out when comparing this to figure 4.1 is that charging now takes place at 40% RH. But, for the lowest available humidity level (20% RH) there is still no charging. Another observation that really stands out is the case with 98% RH. There the charging occurs so quickly that after only 15 minutes the surface is pretty much saturated at 2.5 kV. This is a significant increase compared to the negative case where the surface potential only reached about 1 kV at that time instant. The increased charging is consistent throughout all tested humidity levels.

Regarding the emerging curve shapes, one can see that the 90% RH case really catches the eye. There, the growth appears not only right beneath the electrode as expected but also slightly to the left at a much lower rate. As there are two distinct regions of charge growth, it can not be explained by surface conduction as that would lead to a gradual decrease of the surface potential from the center. Instead, it is believed that this secondary charged region is caused by a local field enhancement on the electrode high enough to act as a source of charge. Judging from where it is located (about 1 cm from the center), it seems reasonable to assume that its source is somewhere around the joint of the smaller field grading electrode, indicating improper shielding. Also, the fact that it does not appear for the other cases suggests that there is some degree of randomness associated with its location. This observation motivates one to investigate the potential on the entire surface—not just for a single line—more on this in the next section. Lastly, note that the surface potential for the 70% RH case now reaches up to 1.5 kV where it then starts to become asymmetric. This is further evidence that surface conduction indeed becomes significant around that voltage level.

By processing the data in the same manner as for the negative polarity, the dynamics of the positive charging can be achieved plus its variation with humidity. More specifically, converting the surface potential curves into surface charge density curves and then integrating to get line charge densities. This is displayed in figure 4.7 where there are a few noteworthy observations to be made, one of which is the extremely high initial charging rate at 98% RH where the slope is almost completely vertical. As can be seen, this results in the surface becoming close to saturation after about 0.5 hours where the charging rate decreases drastically. However, since surface conduction is not negligible here, the charging still continues but at a rate that is limited by the rate at which charge is moved away from the center. This then allows

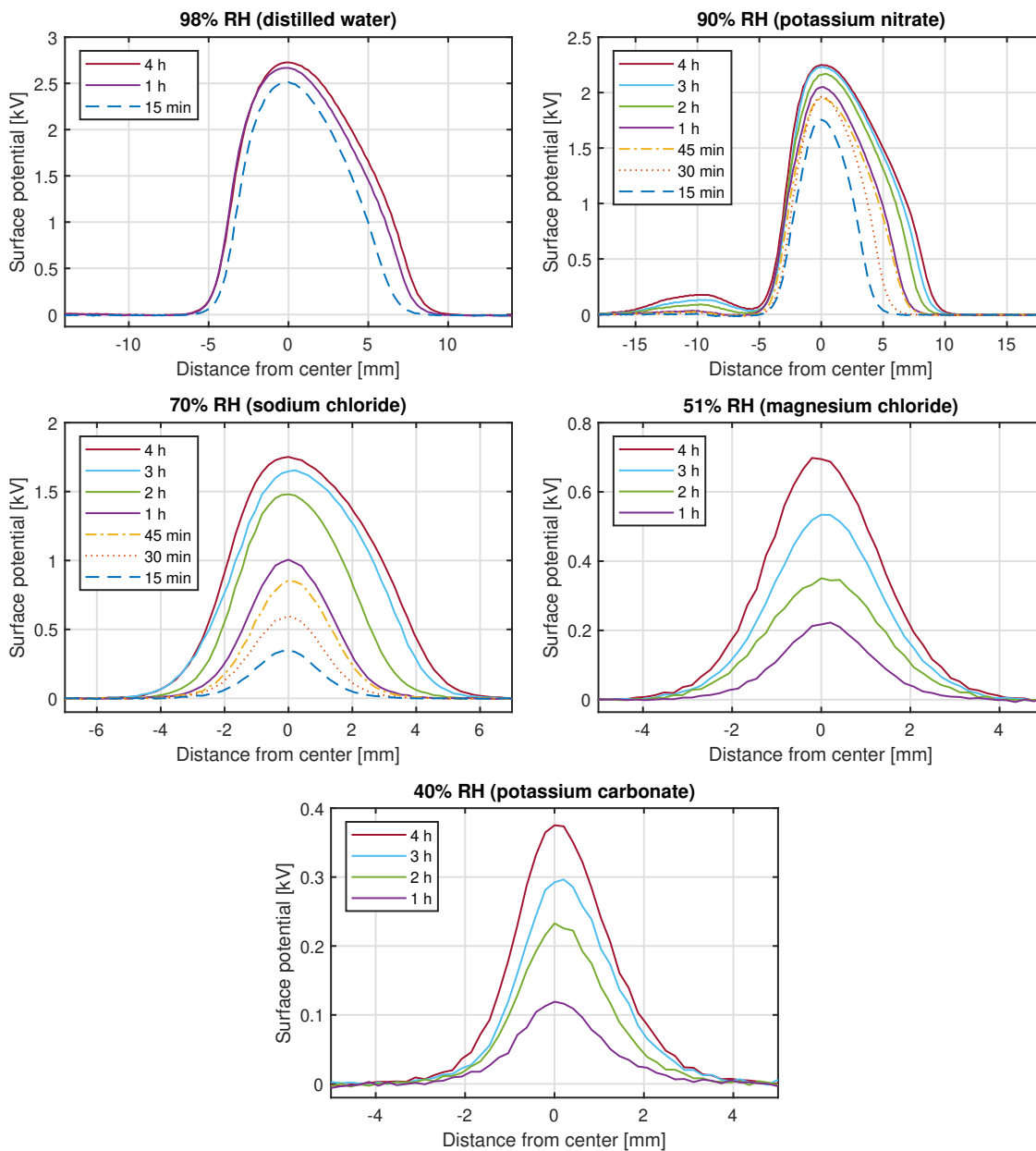


Figure 4.6: Measured surface potential of the positively charged sample along a single line through its center at different time instances and relative humidity levels.

for more charge to accumulate, preventing the surface from ever becoming fully saturated. Note that without any significant surface conduction, the line charge density would instead tend towards a vertical asymptote whose value corresponds to the amount of charge needed to fully saturate the surface. Another important observation is the fact that at 90% RH the slope is substantially greater than for 98% RH after the so-called knee point. This implies that surface conduction is more prevalent in the 90% RH case. An explanation for this inconsistency could be that there are other charged regions on the sample which are not detected here. The electric field from these charged regions could then increase the surface conduction in some areas while decreasing it in others depending on where they appear on the sample. This observation provides yet another reason as to why it is of interest to scan the entire sample.

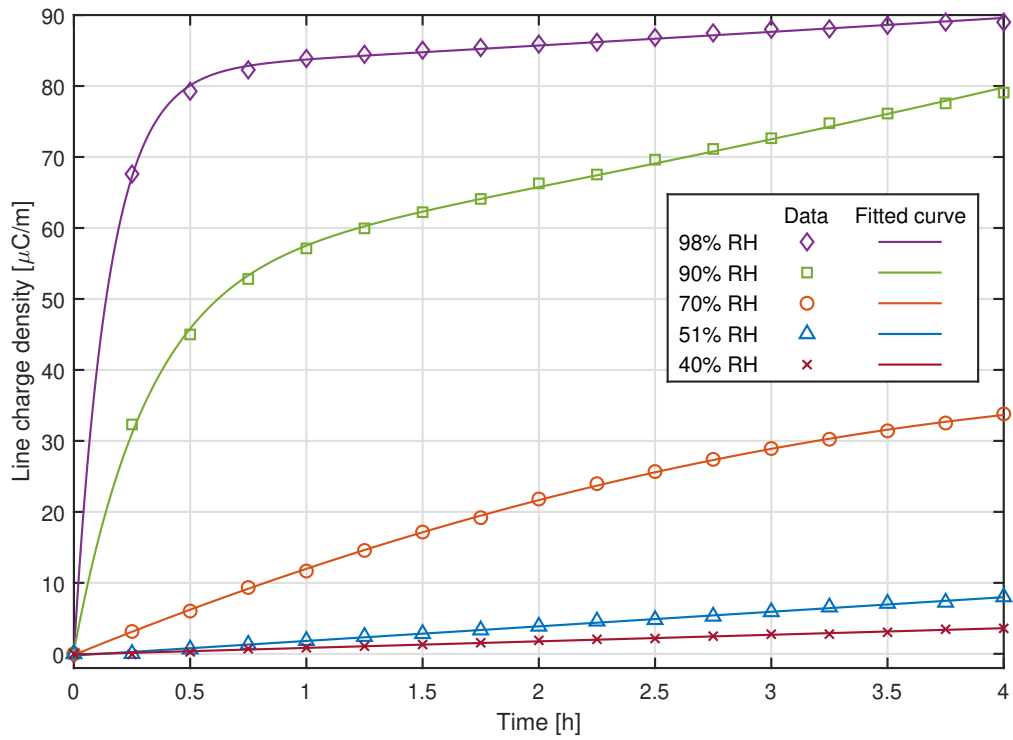


Figure 4.7: Positive charging dynamics for the different humidity levels.

Continuing with the analysis, the initial charging rate (surface current density) is calculated for the humidity levels in question and is plotted in figure 4.8 as a function of relative humidity. As one can see, the relation between initial current and relative humidity is still an exponential on the form ae^{bx} but with different values for the constants ($a = 0.0002055$, $b = 0.137$).

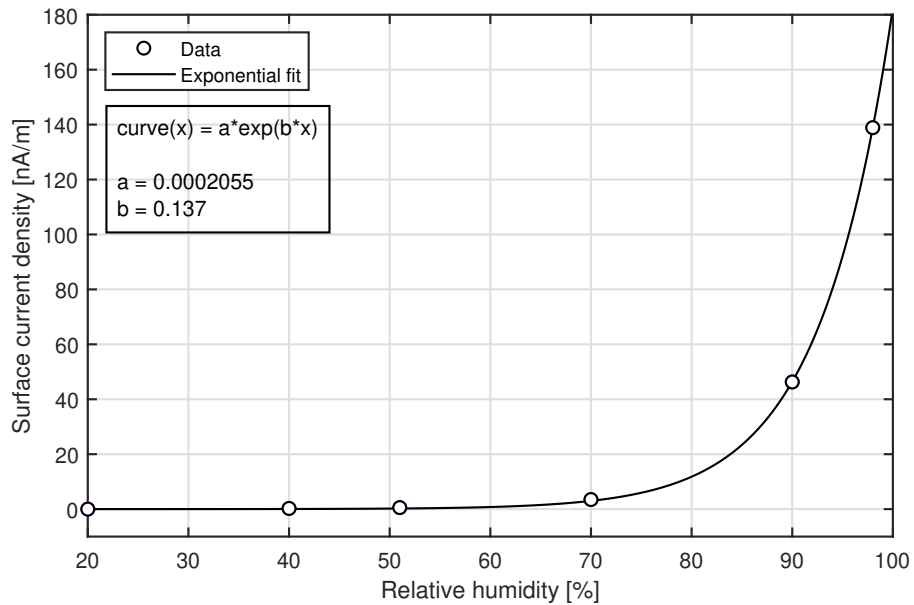


Figure 4.8: Initial charging rate as a function of relative humidity for a positive applied voltage.

As a result, the variability in the higher humidity levels is greater compared to the case with a negative polarity. This clearly shows that the polarity has a significant impact on the rate at which charge carriers are generated. Although, it is not clear why this polarity dependence exists, one can speculate that it has something to do with the formation and emission of adsorbed water ion clusters. It is believed that a positive polarity emits protonated water ion clusters $\text{H}^+(\text{H}_2\text{O})_n$ while a negative polarity emits hydroxide water ion clusters $\text{OH}^-(\text{H}_2\text{O})_n$ [5]. It therefore seems that the process which turns a hydroxide molecule into a water cluster ion and then releases it takes a substantially longer time than for the single hydron. This actually makes sense since the hydron (proton) is a lot smaller than the hydroxide and can therefore more easily drift through the adsorbed layer of water. Furthermore, the proton is symmetric unlike the hydroxide which could make it better at attracting nearby water molecules since its spacial orientation does not matter.

4.2 Charge distribution

As stated previously, there is plenty of motivation for investigating the surface potential/charge distribution of the entire sample. This mainly stems from a suspicion of there being other charged regions outside of the measured line which could play a role in the observed asymmetric charging patterns. Since the degree of asymmetry tends to increase with relative humidity, it is here sufficient to study only the highest humidity level. Accordingly, the surface potential of the entire sample after 4 hours of charging at 98% RH for both polarities is depicted in figure 4.9. It is constructed by first measuring along 37 individual lines separated by 2.5 mm—spanning the whole surface—and then interpolating the missing data using a cubic interpolation method in Matlab. Also shown in the figure are contour maps for respective polarity to provide a better perspective of exactly how the potential is distributed.

As can be observed, there are actually local regions of charge besides the obvious one directly below the electrode. In this case, two small ones located south-west of the center for the negative polarity, while for the positive polarity a small region appears to the west of the center and another much larger region to the north of it. This proves that the locations at which they appear is rather inconsistent. The fact that the regions are much larger for the positive polarity can most likely be attributed to the associated greater charging rate. Why these appear in the first place is believed to be because of defects in the electrode setup, such as improper shielding of sharp edges located in the various joints which then give rise to high electric fields. Ideally, one ought to use a solid piece of metal without any joint, but with that comes other practical problems such as how to securely mount and energize it. Why the location at which they appear is inconsistent, however, is as of yet unknown. This just goes to show how sensitive these types of long term charging experiments are to minor defects as well as initial conditions.

Also, it can be seen that charge tends to spread in different directions for the two presented cases, namely, towards the north-east for the negative polarity and towards the south-east for the positive. These directions are opposite of where the additional charged regions are located, indicating that they indeed play a role in the asymmetry of the surface conduction by affecting the tangential electric field. This can be used to explain why the surface conduction is more prevalent for 90% RH compared to 98% RH in figure 4.7. Simply put, the majority of the surface conduction occurs along a different line than the measured one. Consider the contour map

for the positive polarity; there, the measured line is along the x-axis while most of the surface conduction occurs towards the south-east and is therefore not detected.

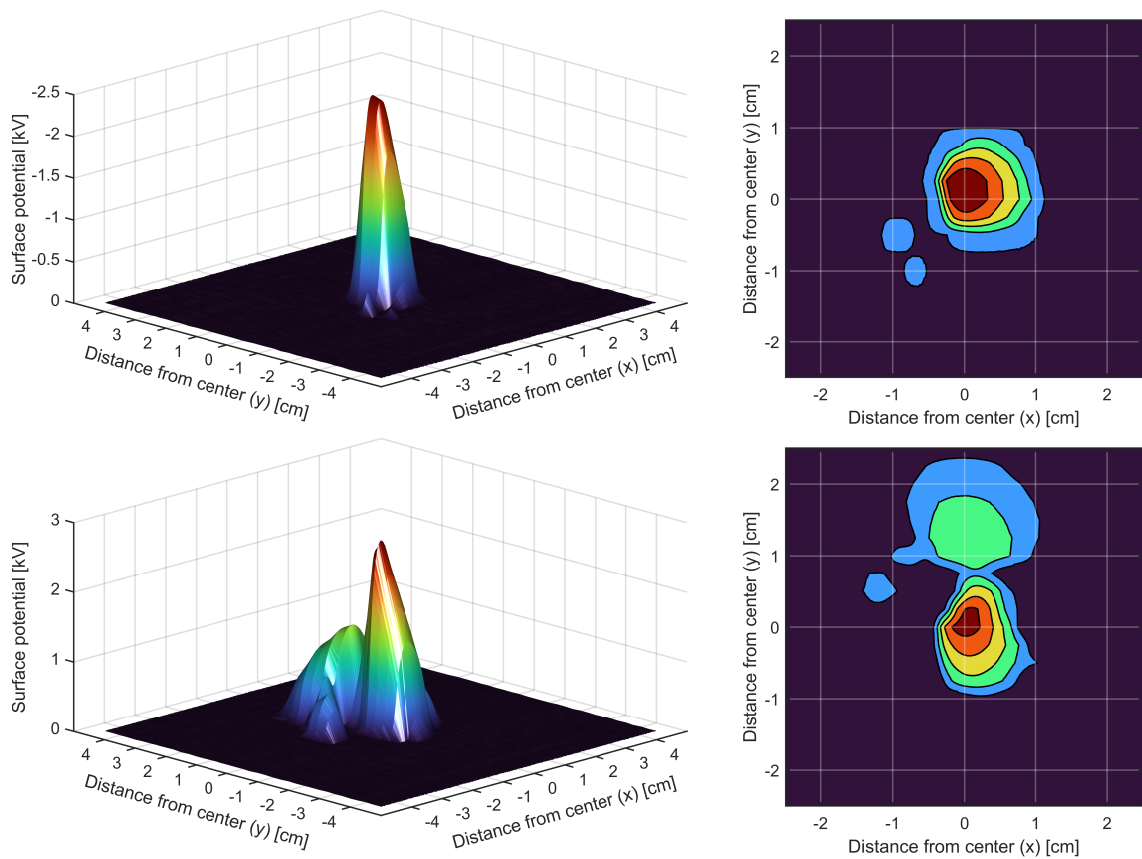


Figure 4.9: Surface potential distribution across the entire sample along with corresponding contour map after 4 hours of charging at 98% RH for both a negative polarity (upper panels) and positive polarity (lower panels).

Despite all the efforts made to achieve symmetrical charging, such as energizing the electrode via a vertical copper rod, placing the high voltage cable outside of the box far away from the sample, using various methods for field grading on the electrode itself; it still was not enough. Although these changes did make a significant improvement, the biggest improvement to the charge distribution was observed after polishing the ground electrode and the field grading ring as well as filing down the threads on the screw holding the electrode arrangement. However, because these three changes were done at the same time—due to time limitations—it is not clear which one of them had the biggest impact. Before any major improvements had been made to the setup, the asymmetry was so pronounced that even the primary charged region did not appear directly below the electrode. In fact, it was offset by at least a whole centimeter. Therefore, the importance of a sophisticated experimental setup can not be stressed enough for these types of long term surface charging experiments. For short term experiments, however, such as charging with corona discharges where the surface becomes saturated within a matter of seconds, a very rough setup can generally be used without causing significant asymmetry.

5 Conclusions

This thesis work aimed at studying the humidity dependence of surface charge accumulation on a flat teflon sample under HVDC conditions below the onset voltage for electron avalanches. For this purpose, an experimental setup was developed that allowed for surface charging and surface potential measurements as well as regulating and monitoring relative humidity. In addition to this, the electron avalanche onset voltage was determined for the given electrode arrangement using computer simulation and was found to be around 5 kV. To ensure that avalanches did not develop, a voltage of 4 kV was used throughout the experiments.

The experimental results showed that the initial charging rate increased exponentially with relative humidity for both polarities, confirming that there exists a charge carrier generation mechanism whose rate is dependent on humidity. Furthermore, the charging rate was substantially higher for a positive applied voltage, proving that the mechanism is also highly polarity dependant. An attempt was made to explain this mechanism by assuming that the generated charge carriers were water ion clusters emitted from water vapor adsorbed onto the electrode. As this is a surface phenomena, the exponential dependence could then be explained by the fact that the amount of adsorbed water exhibits an exponential increase with humidity as well [21]. It was also found that for a negative polarity, no significant charging occurred at 40% RH and lower while for a positive polarity the charging stopped at 20% RH. This shows that the contribution of surface charge from natural ionization of air was negligible, but also that a thinner layer of adsorbed water was required for emitting positive water cluster ions.

Regarding the charge distribution, it was established that there were other charged regions besides the one directly below the electrode which grew at a considerably slower rate. This was explained by suggesting that there were other parts of the electrode where the field was sufficiently high to act as a second source of charge carriers. Simply put, due to a non-ideal electrode setup with insufficient shielding. Moreover, the locations of these additional charged regions were inconsistent, suggesting that they were highly sensitive to initial conditions. It was also observed that the charging eventually became asymmetric once the surface potential had reach a magnitude of around ± 1.5 kV. This is believed to be primarily because of the additional charged regions becoming large enough to enhance the tangential electric field in certain places, locally increasing surface conduction which results in an asymmetric distribution. This was observed when studying the total charge distribution, the majority of surface conduction occurred along a direction that was opposite of where the additional charged regions were located.

6 Future Work

As there were clear imperfections in the experimental setup presented in this thesis, an obvious way to continue the work would be to repeat the experiments using a more sophisticated setup. In particular, a setup where humidity and temperature can be regulated more precisely and where the charging is done with a defect-free electrode, that is, a solid smooth metal without joints. This would yield more accurate results which could serve as a basis for the development of a physical model describing the dynamics of surface charging. Such a model with predictive capabilities can then be implemented in Comsol Multiphysics to systematically study the charging phenomena for various geometries, field inhomogeneity and field levels; further improving the understanding of underlying physical phenomena for charge carrier generation, transfer and accumulation.

Another suggestion for future work based on input from Leif Nyholm—a professor in electrochemistry in Uppsala university—is to measure the pH-value on the electrodes after charging. This could provide further evidence towards the proposed charge carrier generation mechanism that emits water ion clusters. Since water ion clusters of opposite polarity to that which is being used are believed to reside on the electrode surface, they could potentially be detected with a so-called pH-strip by directly applying it to the electrode and letting it soak up the adsorbed water, thereby indicating the pH-value. Since pH is a logarithmic scale describing the concentration of H^+ ions, a negative applied voltage is expected to result in the highest pH-value as it is believed to cause $H^+(H_2O)_n$ to settle on the electrode surface. Also, in the case that the electrode is not sufficiently wet, the pH-strip can be soaked in distilled water before applying it to the electrode. Alternatively, a very small drop of water could be put on the electrode and then have the pH-strip applied to the same place.

The experimental results showed substantial surface conduction which was attributed to additional charged regions altering the tangential electric field, but also to an increasing relative humidity. However, it is not clear to which degree these two factors influence surface conduction. Hence, it is of interest to quantify the humidity dependence of surface conductivity for polymeric materials. For this, a setup for surface conductivity measurements under different humid conditions needs to be developed. But this can be quite tricky since conventional measuring techniques of surface conductivity either encapsulates the sample in a “measuring box” or employs a closed two-ring electrode probe over the sample’s surface, preventing it from adsorbing moisture. As such, a new creative method for surface conductivity measurements which keeps the sample exposed to the surrounding air needs to be developed for this purpose.

References

- [1] P. Fairley, “China’s state grid corp crushes power transmission records,” *URL: <https://spectrum.ieee.org/energywise/energy/the-smarter-grid/chinas-state-grid-corp-crushes-power-transmissionrecords>*. accessed on 2021-07-28.
- [2] R. Hackam, “Outdoor HV Composite Polymeric Insulators,” *IEEE Transactions on Dielectrics and Electrical Insulation*, vol. 6, no. 5, pp. 557–585, 1999.
- [3] S. Kumara, *Electrical Charges on Polymeric Insulator Surfaces and their Impact on Flashover Performance*. Chalmers University of Technology, 2012.
- [4] P. D. Mundim, H. Löfås, N. Lavesson, and V. Bandapalle, “Ion Current Measurements in Air for HVDC Applications,” in *2018 IEEE 2nd International Conference on Dielectrics (ICD)*, pp. 1–4, IEEE, 2018.
- [5] H. R. Carlon, “Electrical properties of atmospheric moist air: A systematic, experimental study,” tech. rep., CHEMICAL RESEARCH DEVELOPMENT AND ENGINEERING CENTER ABERDEEN PROVING GROUND MD, 1988.
- [6] A. Mikiver, “Measurements of Air Ion Concentrations and Electric Field Strengths for HVDC Applications,” 2017.
- [7] A. Hirsikko, *On Formation, Growth and Concentrations of Air Ions*. Helsingin yliopisto, 2011.
- [8] U. Hörrak, *Air Ion Mobility Spectrum at a Rural Area*, vol. 15. Tartu University Press, 2001.
- [9] P. Kolarž, M. Gaisberger, P. Madl, W. Hofmann, M. Ritter, and A. Hartl, “Characterization of ions at Alpine waterfalls,” *Atmospheric Chemistry and Physics*, vol. 12, no. 8, pp. 3687–3697, 2012.
- [10] N. R. Council, G. S. Committee, *et al.*, *The Earth’s electrical environment*. National Academies Press, 1986.
- [11] J. Kuffel and P. Kuffel, *High Voltage Engineering Fundamentals*. Elsevier, 2000.
- [12] D. K. Cheng, *Field and Wave Electromagnetics*. Pearson Education Limited, second ed., 2014.
- [13] A. Küchler, *High Voltage Engineering: Fundamentals-Technology-Applications*. Springer, 2017.
- [14] L. Greenspan *et al.*, “Humidity Fixed Points of Binary Saturated Aqueous Solutions,” *Journal of research of the national bureau of standards*, vol. 81, no. 1, pp. 89–96, 1977.
- [15] S. Alam, *Surface potential dynamics on insulating polymers for HVDC applications*. Chalmers University of Technology, 2016.

- [16] Y. Späck, S. Kumura, and S. Gubanski, “Charge decay measurements on a polymeric insulation material under controlled humidity conditions,” in *Proceedings of the Nordic Insulation Symposium*, no. 23, 2013.
- [17] M. A. Noras, “Non-contact surface charge/voltage measurements,” in *Trek application note No. 3001*, 2002.
- [18] S. Andersson, A. Sonesson, O. Svahn, and A. Tullberg, *Gymnasie KEMI 1*. Liber AB, fourth ed., 2012.
- [19] H. Frank, “Theory and Molecular Models for Water,” *Advances in chemical physics*, vol. 31, p. 1, 1975.
- [20] S. Andersson, U. Ellervik, L. Rydén, A. Sonesson, O. Svahn, and A. Tullberg, *Gymnasie KEMI 2*. Liber AB, sixth ed., 2014.
- [21] R. Hassel and N. Hesse, “Characterization of Water Adsorption and Absorption in Pharmaceuticals,” tech. rep., TA Instruments, 2007.
- [22] C. J. Rothfuss, V. K. Medvedev, and E. M. Stuve, “Temperature and field dependence of protonated water cluster emission from field adsorbed water layers on platinum,” *Surface science*, vol. 501, no. 3, pp. 169–181, 2002.
- [23] “TEFLON,” URL: https://catalog.wshampshire.com/Asset/psg_teflon_ptfe.pdf. accessed on 2021-07-28.
- [24] E. Seran, M. Godefroy, E. Pili, N. Michielsen, and S. Bondiguel, “What we can learn from measurements of air electric conductivity in 222rn-rich atmosphere,” *Earth and Space Science*, vol. 4, no. 2, pp. 91–106, 2017.
- [25] T. Ohmi, S. Sudoh, and H. Mishima, “Static charge removal with IPA solution,” *IEEE Transactions on semiconductor manufacturing*, vol. 7, no. 4, pp. 440–446, 1994.